Universidade de São Paulo
Instituto de Física

Espectroscopia de força atômica em células de melanoma e queratinócitos

Nataly Zaribeth Herrera Reinoza

Orientadora: Profa. Dra.Maria Cecília B. S. Salvadori

Dissertação de mestrado apresentada ao Instituto de Física da Universidade de São Paulo, como requisito parcial para a obtenção do título de Mestre(a) em Ciências.

Banca Examinadora:
Profa. Dra. Maria Cecília B. S. Salvadori - Orientadora (IFUSP)
Prof. Dr. Tharcisio Citrangulo Tortelli Junior - ICESP
Prof. Dr. Vladimir Jesus Trava Airoldi - INPE

São Paulo
2019

FICHA CATALOGRÁFICA
Preparada pelo Serviço de Biblioteca e Informação do Instituto de Física da Universidade de São Paulo

Herrera Reinoza, Nataly Zaribeth

Espectroscopia de força atômica em células de melanoma e queratinócitos. São Paulo, 2019.

Dissertação (Mestrado) – Universidade de São Paulo. Instituto de Física. Depto. de Física Aplicada

Orientador: Profa. Dra. Maria Cecília Barbosa da Silveira Salvadori
Área de Concentração: Física

Unitermos: 1. Microscopia de força atômica; 2. Melanoma; 3. Queratinócitos; 4. Módulo de elasticidade; 5. Force volume.

USP/IF/SBI-021/2019

University of São Paulo
Physics Institute

Atomic force spectroscopy in melanoma and keratinocytes cell

Nataly Zaribeth Herrera Reinoza

Supervisor: Prof. Dr. Maria Cecília B. S. Salvadori

Dissertation submitted to the Physics Institute of the University of SÃ£o Paulo in partial fulfillment of the requirements for the degree of Master of Science.

Examining Committee:
Prof. Dr. Maria Cecília B. S. Salvadori - Supervisor (IFUSP)
Prof. Dr. Tharcisio Citrangulo Tortelli Junior - ICESP
Prof. Dr. Vladimir Jesus Trava Airoldi - INPE

São Paulo
2019

A Nacaré, Isabella y Ricardo.

Acknowledgements

À Prof. Dra. Maria Cecilia B. S. Salvadori pela oportunidade e confiança para trabalhar no seu laboratório. Também sou grata por sua paciência, encorajamento, críticas constructuivas, orientação e amizade.

Ao Prof. Dr. Roger Chammas que foi parte crucial nesta pesquisa com seus comentários perspicazes, expêriencia e inúmeros conhecimentos compartilhados., além de fornecer as amostras estudadas.

Ao pessoal do Laboratório de Oncologia Experimental do "Instituto do Câncer do Estado de São Paulo Octavio Frias de Oliveira" (ICESP) por tudo o suporte para a realização deste trabalho, assim como o fornecemento das amostras. Especialmente ao Dr. Tharcisio Citrangulo Tortelli Junior, pela paciência e o conhecimento compartilhado nesta área totalmente nova para mim, sempre tirando todas as minhas dúvidas.

À Dra. Fernanda de Sá Teixeira pelo suporte técnico para o desenvovimento do projeto. Gente fina, sempre receptiva e disposta a ouvir minhas dúvidas. Adorei trabalhar perto de você.

Aos integrantes do Laboratótio de Filmes Finos, Leonardo, Wagner, Roman, Raissa e Natalia, pelas conversas diárias que fizeram o trabalho mais agrável, pelo apoio e incentivo constante. Todos foram essenciais para o desenvolvimento deste trabalho.

À Dra. Luciana Ramos por ter se interessado por este trabalho, ter lido em detalhes o texto e ter dado contribuições maravilhosas para o seu aperfeiçoamento.

A mi mamá Nacaré, que a pesar de estar a unos 4000 km de distancia, es la persona que más cerca siento. Gracias por siempre velar que siga el camino correcto.

A Ricardo por siempre creer y confiar en mi, alentandome cada día y acompañadome en mis mejores y peores momentos. Gracias por incentivarme a seguir adelante a pesar de las adversidades.

A Raissa por brindarme su confianza, cariño, apoyo y amistad. Gracias por tantos momentos compartidos, por abrirme las puertas de tu casa y también las de tu corazón.

À Coordenação de Aperfeiçoamento de Pessoal de Nível Superior - Brasil (CAPES)- Código de Financiamento 001.

Ao Consejo Nacional de Desarrollo Científico y Tecnológico (CNPq) pelo financiamento parcial do mestrado. Nº de processo 132785/2017-0.

À Fundação de Amparo à Pesquisa do Estado de São Paulo (FAPESP) pelo financiamento do projeto 95/5651-0.

À Universidade de São Paulo e à pós-graduação do Instituto de Física pelas oportunidades oferecidas e pela formação de qualidade.

"¿Donde desearia vivir?
Donde vivo, en mi tierra; desventurada como es, imperfecta como es. Porque es donde naci, fui niño, tuve ilusiones, quise transformar el mundo, amé y sufri. Y porque a una tierra nos unen entrañablemente no solo sus felicidades y virtudes sino - y sobre todo - sus tristezas y precariedades."
Ernesto Sabato.

Resumo

Neste trabalho, utilizamos espectroscopia de força atômica para obtenção do módulo elástico de células fixadas de melanoma e queratinócitos, com o objetivo de determinar as condições iniciais de estudos a serem realizados futuramente de culturas de células confluentes do mesmo tipo. As linhagem celulares utilizadas foram as células HaCaT e as células de melanoma WM1366, sendo a última derivada de um melanoma de crescimento radial sendo analisadas tanto as células parentais (células WM1366 shSCR) e as células WM1366 silenciadas com galectina-3 (WM1366 shGal3).

As células foram localizadas e imageadas no modo AFM contato em meio líquido. Curvas de força adquiridas na região central das células foram utilizadas para determinar o módulo elástico, a partir do modelo de contato hertziano por uma ponta piramidal, permitindo estabelecer um padrão para comparação entre células normais e cancerígenas. Verificou-se que a célula de melanoma exibe menor módulo de elasticidade (21.8 ± 0.5 kPa) do que as células de queratinócitos (31.9 ± 0.4 kPa) . Para as células WM1366 shGal3 foi encontrado um módulo elástico de $16,1 \pm 0,6$ kPa. Portanto, verificou-se que, para grandes profundidades de indentação, é possível distinguir entre a mesma linhagem de melanoma, células que apresentam alterações gerais na organização do citoesqueleto induzidas pela presença ou ausência da proteína galectina-3.

Por outro lado, para detectar variações locais do módulo elástico ao longo da célula e identificar regiões subcelulares, caracterizadas por rigidez específica associada a estruturas locais, foram obtidos mapas de elasticidade nos quais uma única curva de força é adquirida em cada posição da sonda. Para interpretar estes mapas, a célula foi dividida em regiões de diferentes alturas e curvas de cada seção de altura foram analisadas e representadas em histogramas, ajustadas pela função de distribuição binomial. Observou-se que o gradiente de módulo de elasticidade em células da região nuclear em direção à periferia celular é mais acentuado em células desprovidas de galectina-3 do que em células parentais. O aumento do módulo de elasticidade na região pericelular das células desprovidas de galectina-3 sugere que a organização da matriz extracelular nestas áreas é diferente das observadas em torno das células HaCaT e shSCR WM1366.

Palavras-chaves: AFM, melanoma, queratinócitos, módulo de elasticidade, *force volume*.

Abstract

In this work, we used atomic force spectroscopy to obtain the elastic modulus of melanoma and keratinocytes fixed cells, with the purpose to determine the initial conditions for studies of confluente cultures of these cells in the future. The cell lines used were HaCaT cells and WM1366 melanoma cell, the last one is derived from a radial growth melanoma and both were analyzed, parental WM1366 cells (WM1366 shSCR cells) and galectin-3 silenced WM1366 cells (WM1366 shGal3).

Cells were located and images of them were obtained by AFM contact mode under liquid conditions. Single force curves acquired in the central region of cells were used to determine the elastic modulus by the Hertzian contact model for the pyramidal tip, allowing to establish a comparison patter between cancer and normal cells. It was found that the melanoma cell ($21.8 \pm 0.5\ kPa$) exhibit smaller elastic modulus than keratinocytes cells ($31.9 \pm 0.4\ kPa$). For WM1366 shGal3 was found a elastic modulus of $16.1 \pm 0.6\ kPa$, therefore, we found that for large indentation depth it is possible to distinguish between the same melanoma cell line, which represents general alterations in the organization of the cytoskeleton induced by the presence or absence of the galectin-3 protein.

On the other hand, to detect local elastic modulus variations along the cell and to identify subcellular regions characterized by specific stiffness associated with local structures, we took elasticity maps in which a single force curve is acquired in each probe position. In order to interpret these maps, the cell was sliced into several different heights, curves of each height section were analyzed and represented in histograms, adjusted by the binomial distribution function. It was observed that the gradient of elastic modulus in cells from the nuclear region towards the cell periphery is more pronounced in cells devoid of galectin-3 than parental cells. The increased elastic modulus in the pericellular region of cells devoid of galectin-3 suggests that the organization of the extracellular matrix in these areas is different than those observed around HaCaT and shSCR WM1366 cells.

Key-words: AFM, melanoma, keratinocytes, elastic modulus, force volume.

List of Figures

List of Tables

Contents

1 Introduction

Cancer occurs when normal cells undergo a process called malignant transformation, a progressive loss of proliferation control at the cellular level, caused by genetic or epigenetic alterations in the genome of parente cells, that are shared by daughter cells. These cells can spread to other regions of the body in process called metastasis. Skin cancer is the most common of all human cancers and there are three major types: basal cell carcinoma (BCC), squamous cell carcinoma (SCC), and melanoma [1], being the last one the most aggressive and lethal skin neoplastic [1] disorder. Melanoma is originated from the malignant transformation of the melanocytes, which are located in the basal layer of the epidermis, and produce and transport melanin, responsible for the pigmentation of our skin, hair and eyes. In Brazil, according to the "Instituto Nacional de Câncer José Alencar Gomes da Silva"[2], 1500 people die every year due to melanoma and it is estimated that 6000 new cases will be diagnosed during 2018. Despite of advances in melanoma treatment, mortality from this kind of cancer is still increasing, establishing as one of the cutaneous diseases with greater growth in this century [3]. Therefore, it is necessary to develop prognostic biomarkers that can differentiate between malignant and non-malignant skin lesions and that can identify melanoma patients with high-risk primary lesions to facilitate greater surveillance [4]. In this way, the discovery of biomarkers and their application, together with traditional cancer diagnosis could improve early diagnosis, which is vital for the patient.

Several studies have reported that cancer transformation introduces significant changes in the cell structure and behavior. Such alterations can affect cell growth, morphology, cell-to-cell interaction, cell membrane, extracellular matrix and organization of the cytoskeleton [5, 6]. Hence, these differences may also induce changes in cell mechanical properties, which can be described through the elastic modulus. The elasticity response of biological system have been explored using different experimental techniques such as micropipette aspiration (MA) [8], optical tweezers (OT)[9], magnetic tweezers (MT)[10], force traction microscopy (TFM)[12], magnetic twisting cytometry (MTC)[11] and atomic force microscopy (AFM). Among these techniques, the use of AFM to probe the

[1] Neoplasia is a term used to designates cellular alterations that cause an exaggerated cell growth, i. e. abnormal cellular proliferation, without control, which leads to the reduction or loss of the differentiation capacity of the cell.

mechanical properties of biological systems give us the possibility to obtain measurements of cell morphology in physiological close conditions with high spatial resolution, as well as, to study the elastic modulus in a local way by means force spectroscopy. Beside that, AFM is a technique in which the interaction force between the probe an the sample surface is measured using a very simple experimental setup. To determine the elastic modulus by means AFM, the probe is used to induce a local deformation on the cell surface, applying force in the range of 10^{-12} to 10^{-6} N, which is an optimal interval to elasticity cell studies, because higher forces may produce damage in the sample and lower forces may provide non-reliable measurements.

The aim of this work is to determine the initial conditions for studies of confluente cultures of keratinocytes cells with melanoma cells, modeling the conditions observed in situ melanomas, i.e., the condition where malignant melanoma cells are still interacting with keratinocytes in the early phases of melanoma evolution. Another aspect is to verify the possibility of obtaining a biomarker of the disease malignancy. For this purpose, we will use two cell lines, keratinocyte cells (HaCaT cell line), and the WM1366 melanoma cell line. WM1366 cell was derived from a radial growth melanoma, i.e. they derive from a stage when tumor cells still interact closely with keratinocytes. Changes in the expression of a variety of molecules define the acquisition of a more invasive phenotype. Among these alterations is progressive lost of galectin-3 expression (for a review, see Cardoso et al. [13]). Therefore, here we will use both parental WM1366 cells (WM1366 shSCR cells, which express galectin-3) and galectin-3 silenced WM1366 cells (WM1366 shGal3), as described elsewhere (Bustos et al. [14]). In order to quantify the elastic modulus of these cells, AFM operating in force spectroscopy mode will be used. Single force curves acquire in its central region will be used to determine the elastic modulus allowing to establish a comparison patter between cancer and normal cells. On the other hand, to detect local elastic modulus variations along the cell and to identify subcellular regions characterized by specific stiffness associated with local structures, we will be taken force volume in which a single force curve is acquired in each probe position.

This master dissertation is organized in the following way: *chapter* one is the present introduction, together with the fundamentals of the problem and the state of the art, which will be given in the following sections, it also introduces the basic information about cell lines, terms used in biomechanics of cell and the significance of cellular deformability properties. *Chapter* two relates the materials used in this work, and presents the fundament and working principle of the AFM technique, as well as, experimental features. In *Chapter* three results are shown and discussed and in *Chapter* four conclusions and perspective for continuing of this work are given.

1.1 Fundamentals and the state of the art

Eukaryotic cells are delimited by a plasma membrene, which is a semipermeable barrier that separates the interior of the cells from its environment, and also regulates the communication between cells. Inside the plasma membrane are the cellular nucleus and the cytoplasm. The cytosol is considered the fluid phase of the cytoplasm, which

is composed of about 80% water. The rest corresponds to proteins, metabolites and organelles. Such high percentage of water suggests to consider the cell as a incompressible material [22]. Embedded together with the cytosol is the cytoskeleton that consists of a dynamic and complex network of protein filaments and other associated proteins that provide structural support to the cell and stabilize the cell shape. Besides it participates in various other functions such as intracellular trafficking, cell division, and migration. Outside the membrane is the extracellular matrix that serves as mechanical support to the cell, but also has a unique role in regulating cell morphology, signaling, migration, division, and even differentiation [19].

There are many elements that determine the cellular architecture, its function, behavior, and biomechanical properties. Specifically, the cell body is constantly reorganized by its internal scaffolding, the cytoskeleton network [18]. Several studies have associated the cell deformability, in response to external forces, with the cytoskeleton structure, considering that its elasticity is influenced by the mechanical and chemical environments including cell–cell and cell–extracellular matrix interactions. The cytoskeleton is mainly constituted by three types of filaments: actin filaments, microtubules and intermediate filaments. Each type of filament is distributed throughout the cell in an organized manner, assuming different structures (permanent or transient) during a cell life, in response to internal or external signals, as shown in Figure 1.1. It is important to say that the actin filament have been suggested as the most significant cytoskeleton component for modulating the mechanical properties of cells [19, 20, 21].

The architecture of the cytoskeleton is dependent on the specific concentration, molecular state, and organization of each biopolymer component, which also determines the mechanical deformation characteristics of the cell. Any changes to the cellular architecture will alter the organisms biological processes and/or the mechanical properties. As consequently, different types of cells will have a different cytoskeletal structure, so they will have different mechanical properties. In fact, it has been reported that different diseases cause significant changes in the cellular stiffness as a result of rearrangement of cytoskeletal structure. These observations have also been reported for cancer cells [24]

The mechanical response of any material can be determined through the nature of deformation generated by the external force. This response can be purely elastic, viscoelastic or purely plastic. Purely elastic material has an ability to resist an external force and to return to its original size and shape when the stress is removed. On the other hand, purely plastic materials undergo irreversible changes of shape in response to external forces. The remaining deformation types include a combination of elastic and plastic behaviour, i. e. viscoelastic behaviour. Depending on the value of the external force acting upon the material, different deformation modes may occur. An elastic region, where deformation is reversible, occur up to a certain extent of the strain, the yield strength, where plastic deformation begins. In the case of biological system, in particular the cell that presents a heterogeneous intern structure, the viscoelastic behaviour is verified [33].

In order to simplify the theoretical models and also make a significant characterization of the cell lines, it will be analyzed only the elastic contribution of the cellular mechanical

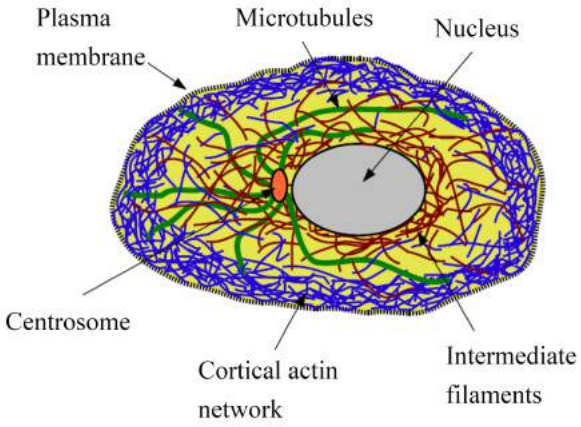

Figure 1.1: A schematic of the typical organisation of the cytoskeletal filaments inside an eukaryotic cell. Each type of filament has distinct mechanical properties, dynamics, and biological roles, but all share certain fundamental features. Actin filaments are the most abundant cytoskeleton elements, which form a meshwork below the plasma membrane. The microtubules start from the center located nearby the nucleus and extend all the way to the actin cortex. The intermediate filaments are concentrated around the nucleus and extend in lower numbers away from the nucleus. Adapted from Pullarkat et al. [19].

response, being quantified by means the elastic module or Young's modulus. In this way, it is possible a direct comparison between populations of cells, which is decisive in determining a possible malignant marker.

The elastic modulus is defined as the ratio of the stress along an axis (described as force per unit area) to the strain along that axis, which is calculated as deformation of the initial length in the range where Hooke's law is working, i.e.,

$$\sigma = E\varepsilon \tag{1.1}$$

where, σ is the applied stress, E is a elastic modulus, which is a material constant and ε is the fractional strain.

Cancer is a disease in which many of the characteristics of normal cell behavior are lost or perturbed, such as growth, morphology and cellular adhesion. Therefore, it is expected that the mechanical resistance maintained by the cytoskeletal network and its organization are altered in cancerous cells in comparison the normal ones [26]. Therefore, research focused on the correlation between cellular structures and the nano-mechanic properties of cells could help in the identification of new malignancy biomarkers. In fact, it has already been demonstrated that cell stiffness can be a marker of the oncological process in several types of cancer [27, 28].

Several techniques have been developed to measure mechanical response to single cells and biological materials. According to Du et al. [23] these techniques can be roughly divided into, methods that probe mechanical properties locally, and methods that deform cells globally. The first category includes techniques such as atomic force microscopy (AFM)[29, 30], magnetic twisting cytometry [10] and cytoindentation [12]. Although these approaches can provide a quantitative mechanical analysis, the biomechanic

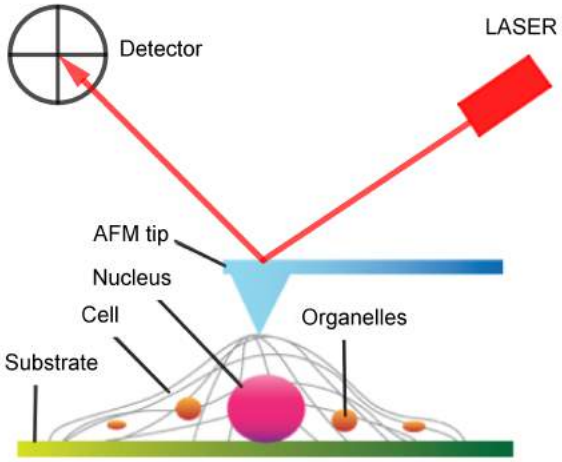

Figure 1.2: Illustration of the AFM experimental setup. Adapted from [28].

response depends significantly on the precise measurement location. As a result, these techniques generally show a large cell-to-cell spread, thus measurements on a significant number of cells are required for statistically meaningful results. Techniques in which cells are deformed globally are laser/optical cell stretching [9] and micropipette aspiration [8]. Many of these techniques are performed on a per-cell basis. Therefore, they require single-cell handling which can make them very tedious and slow (several cells per hour). Furthermore, in many methods it is difficult to control the micro-environment around the cells to be tested. It would be desirable for testing the effect of environment on mechanical properties, or for creating physiologically relevant conditions.

In particular, the AFM has emerged as an ideal tool in the biological materials research ranging from single proteins to living cells [31, 32]. AFM provides topography image with high vertical and lateral spatial resolution, as well as, it gives information about mechanical properties, such as elasticity, friction, or adhesion forces, by means of force spectroscopy mode operation, in close physiological conditions (buffer solutions, in situ, and in vitro). Also, a minimal sample preparation is requited. In Figure 1.2 it is illustrated the basic operating principle of an AFM. Among the first works that focus on the determination of mechanical properties of normal and cancer cells using AFM, it is the one presented in 1999 by Lekka et al. [6]. In this work were studied normal and cancerous human epithelial cell lines, being found that the average elastic modulus values for the cancerous cell were about one order of magnitude lower than the benign cell line. These results were attributed to poorly developed cytoskeletal elements in metastatic cell. Recently, Sobiepanek et al. [34] studied the elasticity behavior of melanocytes (HEMa-LP) and two melanoma cell types (primary RGP WM35 and metastatic A375-P melanoma cells), which were grown on glass coverslips. In Figure 1.3 it is shown topographic images of AFM of HeMa-LP, WM35 and A375-P cells, without revealing significant differences between cell lines. Despite not being found marked morphological differences between the cells studied, using force spectroscopy, it was determined that normal melanocytes have a large rigidity compared to melanoma cells (see histograms in Figure 1.3), which is consistent with that reported by Lekka et al. [6] two decades earlier.

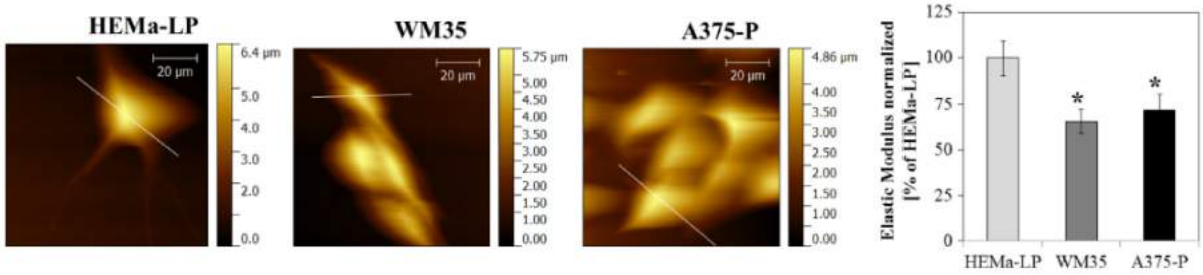

Figure 1.3: Topographic images of living HEMa-LP, WM35 and A375-P cells, acquired in cultured medium with a scan rate $0.7Hz$. The rigidity of living melanoma cells (WM35 and A375-P) is presented as a percentage of change in relation to the melanocytes(HEMa-LP). In order to determine the elastic modulus, force curves were collected from the center of the cells, using $4nN$ as maximum indentation force and $9\mu m/s$ as a speed of indentation. Adapted from [34].

On the other hand, Gostek et al. [35], who focused on the nano-characterization of two different melanoma cell lines with similar morphological appearance but different metastatic potential, namely, WM115 from vertical growth phase (VGP) and WM266-4 derived from metastasis to skin, demonstrated that the elastic modulus value is dependent of the indentation depth and cellular density. Figure 1.4 presents Young's modulus values obtained for indentation depth of $50nm$ (a), $200nm$ (b), and $500nm$ (c) for living melanoma cells grown at low (a single cell) and high density (in semi-confluent monolayer conditions). Fluorescence microscope images are also presented, where it is highlighted that melanoma cells cultured at higher density have displayed occasional partial overlap of cells.

Likewise, Chiou et al. [21] analyzed the effective Young's modulus for MDCK cells as a function of the cellular density and observed similar results. Topographic images of AFM are displayed in Figure 1.5 together with the immunofluorescence images for densities of 5, 50, and 500 $cells/mm^2$. Also the effective Young's modulus for each situation was calculated (see Figure 1.5(b)), indicating that effectively cell-cell interactions affect the mechanical properties.

In addition, this dependence on Young's module on non-tumorigenic and carcinoma prostate cells was studied [36]. In Figure 1.6*(a)* are exhibited the results, evidencing that the influence of neighboring cells on the elasticity measurements will depend on the type of cell. For example, it was found that the Young's modulus increased with the cell density for PZHPV-7 (derived from a healthy gland) and Du145 (brain metastasis), while for LNCaP (lymph node metastasis) and PC-3 (bone metastasis) lines, Young's modulus changes slowly.

Different cellular structures can be probed by varying the indentation depth. The mechanical response for smaller indentations depths is dominated by the filamentous network of actin filaments. On the other hand, larger indentations depths allow probing of cellular regions rich in all cytoskeleton elements and the cellular nucleus. In such case, the overall elasticity of the whole cell can be obtained. Pogoda et al. [36] reports an indentation depth scanning from 200 nm to 1400 nm for two melanoma cell lines, finding that the elastic modulus value becomes approximately constant for indentations greater

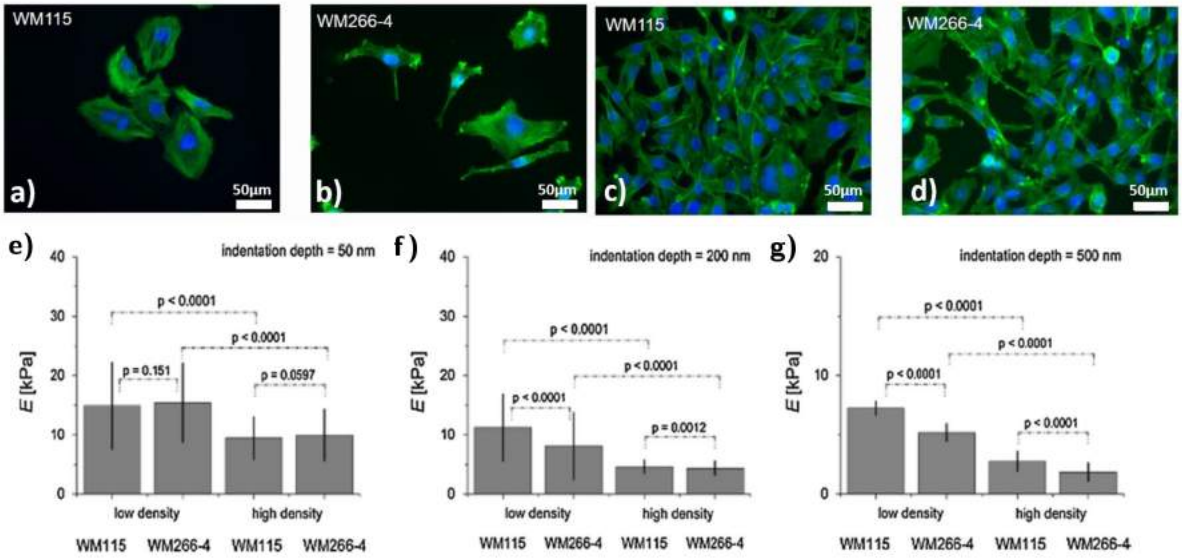

Figure 1.4: Fluorescence microscope images of WM115 and WM266-4 cells (a, b) single cells and in conditions of a semi-confluent monolayer (c, d). The Young's modulus values as a function of cell density and indentation depth (e, f, g). Adapted from [35].

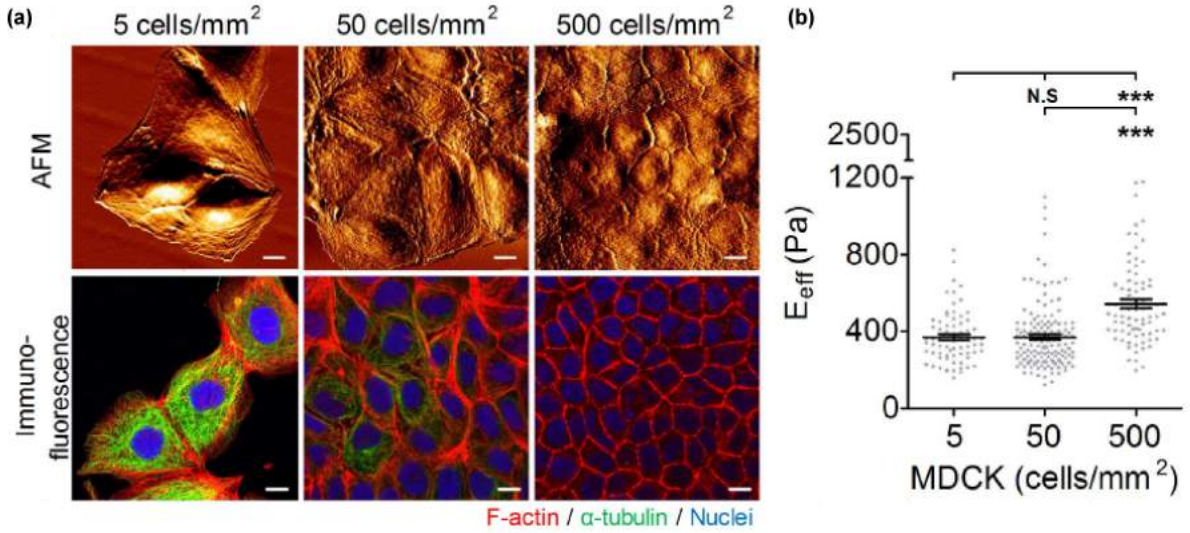

Figure 1.5: (a) AFM topographic images in living MDCK cells (a mammalian cell line) and confocal immunofluorescence images of F-actin (red), α-tubulin (green), and the nucleus (blue) in stained MDCK cells that were cultured at densities of 5, 50, and $500 cells/mm^2$, respectively. (b) Effective Young's modulus expressed as the mean value of the Gaussian distribution that characterizes each of the situations. In this experiment 30 cells were probed for each conditions. The data was acquired in the central region of the cells with 1 nN of applied force and 1 $\mu m/s$ of speed load. Adapted from [21].

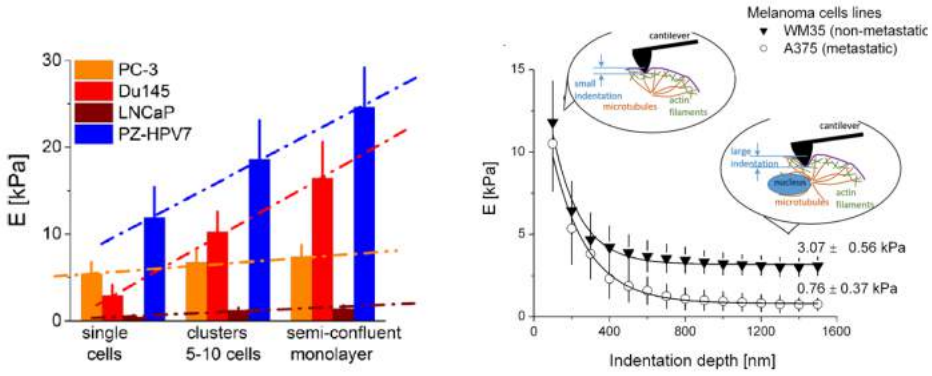

Figure 1.6: (a) Elastic modulus as a function of the cellular density, showing that the mechanical response to the presence of neighbouring cell depends to the type of studied cell. Cell lines analyzed: PZHPV-7 - non-tumorigenic prostate cells, PC-3 – prostatic adenocarcinoma initiated from bone metastasis, Du 145 – metastatic prostate carcinoma from brain metastasis, and LNCaP – metastatic prostate carcinoma established from the left supraclavicular lymph node metastasis. Adapted from [28]. (b) Dependence of Young's modulus as a function of the indentation depth determined for two melanoma cell lines: WM35 (non-metastatic cancer cells from a primary tumor site) and A375 (highly metastatic cells). Each data point represents a mean calculated for a whole cell (i.e. from 140 locations recorded on a single cell). Error bars denote standard deviations. Adapted from [36].

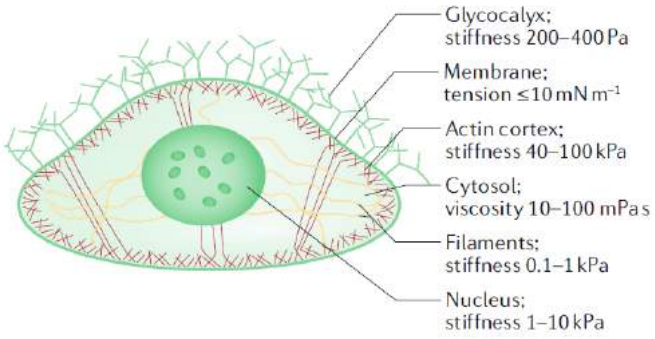

Figure 1.7: To measure these properties, an atomic force microscope tip first indents the $\sim 40-400$ nm- thick soft (stiffness $\approx 200-400$ Pa) glycocalyx surrounding the cell. Upon further indentation, the tip deforms the very soft (tension $\approx 0.1-10$ $mN\ m^{-1}$) and thin ($\sim 5-8$ Nm) cell membrane - its contribution is difficult to measure because it is linked to the subjacent, $100-1000$ nm- thick and much stiffer ($10-100$ kPa) actomyosin cortex. Moreover, while indenting through the meshwork of the cytoskeleton, the probe pushes into the viscous cytoplasm (viscosity $\approx 10-100$ $mPa\ s$) until it encounters stiff filamentous structures (such as actin or microtubuli; stiffness $\approx 0.1-1$ kPa) and/or the nucleus (stiffness $\approx 1-10$ kPa). Adapted from [37].

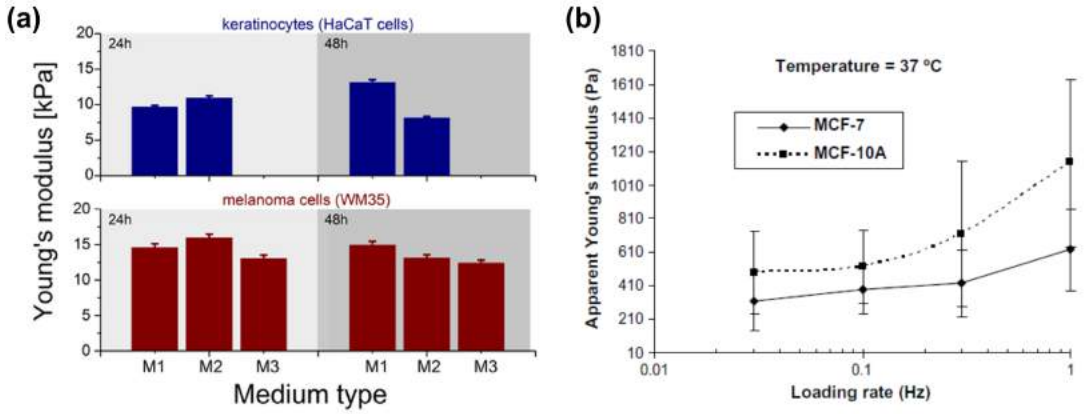

Figure 1.8: (a) Elastic modulus dependency with the surrounding medium for HaCaT and melanoma cells after $24h$ and $48h$ of culture (M1–Dermal Cell Basal Medium; M2–Eagle's Minimum Essential Medium; M3–RPMI 1640 Medium) Adapted from [38]. (b) Plot of the apparent elastic modulus against loading rate for benig (MCF-10A) and cancerous (MCF-7) human breast epithelial cells at $37°C$. Error bars indicate standard deviations. Adapted from [40].

than about 700 nm. These results are shown in Figure 1.6(b). It is important to mention that the authors selected the scanning interval taking into account the substrate effects. In a recent review published by Krieg et al. [37] is shown a schematic representation of an adherent mammalian cell with a summary of the mechanical properties of the cellular structures and compartments, where each cellular region was probed using a particular indentation depth (see Figure 1.7).

The elastic modulus obtained by force spectroscopy manifests another interesting dependencies. Zemla et al. [38] illustrate the influence of culture condition on elasticity of normal HaCaT and melanoma cells, showing that the time of cell culture is equally important as the composition of culture medium. This can be observed in the Figure 1.8(a). The influence of load rate has been demonstrated for prostate [28], bladder [39], breast [40], and blood cells [44], being reported that normal cells are more sensitive to the load rate (the elasticity change is larger) as compared to cancerous ones (see Figure 1.8(b)). In this way, it is essential to stand out that in AFM, it is not possible to directly control the load rate value. Its value can be indirectly modified by changing the speed of indentation (load speed). Also, the Young's modulus value can be affected by instrumental factors as calibration of cantilever spring constant and photodetector sensitivity (for more details see *Chapter two*), as well as by data processing. This includes determination of the contact point between the tip and the cell surface and the mechanical models applied to describe the elasticity cell.

In conclusion, the elastic modulus can be determined using force spectroscopy and the comparison between different cell types is possible, especially for cancer cells, where large alterations of cell cytoskeleton are expected. Due to the wide variety of factors that influence the measurement of force curves and data analysis, an absolute value of Young's modulus is not obtained. However, the exact knowledge of the absolute Young's modulus is not always needed, since effective comparisons can be made when the data are acquired under the same experimental conditions.

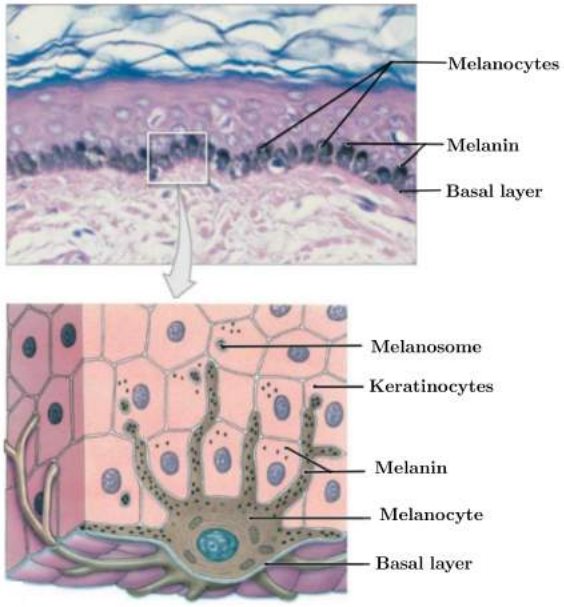

Figure 1.9: Location of melanocytes in the basal layer of the epidermis. Their communication with keratinocytes is represented by the transfer of melanin, pigment that gives color to the skin. Adapted from http://pt-br.biologia-celular-uergs.wikia.com

1.2 Melanoma

Melanoma is the most aggressive form of skin cancer and its incidence has increased in the last years despite of advances in cancer treatment. Melanoma is originated from the malignant transformation of the melanocytes, which are located in the basal layer of the epidermis and produce and transport melanin, responsible for the pigmentation of our skin, hair and eyes.

Basically, the skin is organized in layers. The first of them is the epidermis, which is composed mainly by keratinocytes and melanocytes cells. Keratinocytes represent approximately 80% of epidermal cells and are progressively differentiated controlled by extrinsic and intrinsic events. Melanocytes are melanin-producing cells that are limited especially to the basal layer of the epidermis. Through their prolongations, these cells communicate with the keratinocytes, and this interaction is essential for their differentiation and function. Under normal physiological conditions, melanocytes and keratinocytes form the *Melanin Epidermal Unit* (see Figure 1.9). These cells are aligned in the area of the basement membrane in the ratio 1 melanocyte for every 5 to 8 keratinocytes. Each melanocyte transports melanosomes to approximately 35 keratinocytes from the upper layers of the epidermis through its extensions. As a result, pigmentation of the basal layer and the most superficial layers of the skin occurs, which is mainly responsible for the protection of radiation damage [41].

Under normal conditions, homeostasis [2] determines whether a cell remains quiescent, proliferates, differentiates, or undergoes apoptosis (reviewed in Bissell et al. [42]). Dysregulation of the homeostasis may disturb the balance of the epidermal melanin

[2]Homeostasis is referred to the state of steady internal conditions maintained by living things

unit and trigger a continuous proliferation of the melanocytes, which may lead to the development of melanoma. The hallmarks of solid tumours are uncontrolled proliferation, derangement of cellular and morphological differentiation, invasion, and metastatic spread to distant organs. These characteristics can be in part attributed to alterations in adhesion and communication between neoplastic cells and the normal cells in their immediate microenvironment (reviewed in Hanahan et al. [43]).

Melanoma is characterized by high rate of invasion resulting at various metastatic sites. Usually, this kind of cancer starts as a benign lesion and evolves quickly towards metastatic ones. At the first step, due to oncogenic mutations, melanocytes can transform, through nevus stages, to a flat tumour, growing horizontally (radial growth phase, RGP). It is followed by the acquisition of the ability to invade deeper layers of the skin (vertical growth phase, VGP), what finally leads to the metastasis. The transition, from radial to vertical growth phase, is a crucial step in the melanoma progression. It is correlated with the diversity of alterations that allow for distinguishing between RGP and VGP melanoma cells. Cells derived from vertical growth phase express surface receptors involved in the metastasis. These molecules are a part of the large family of heterodimeric receptors called integrins, that play crucial roles in the regulation of cell survival and migration[45]. Around 60% of melanoma cases had tumour thickness below 1 mm [46]. It is important because they are frequently diagnosed as a non-invasive melanoma and there is a clear need for novel screening strategies. Nevertheless, the incidence of thin metastasizing melanomas is still increasing. It creates an urgent necessity for the determination of other significant criteria and novel melanoma characteristics, molecular as well as mechanical ones, especially on the correlation between their deformability and metastatic potential. It is already well-known, that melanoma cells deformability is related to their metastatic potential. For example, the more invasive melanoma cells were, the larger deformability was observed [47].

The melanoma line will be used in this research is a human melanoma WM (Wistar Melanoma Collection). WM1366 shSCR cells were derived from a radial growth melanoma, i.e. they derive from a stage when tumor cells still interact closely with keratinocytes. Also, it will be studied WM1366 shGal3 cells, which the galectin-3 protein is silenced. These last ones are of interest, because galectin-3 has been identified as a mechanism associated with the progression of melanoma. In fact, it has been found in the literature that thin primary melanomas express more galectin-3 than benign nevus, and this profile is further lost along tumor progression, leading to a decrease of Gal-3 expression in thicker and metastatic melanoma [48, 49]

Galectin-3 (Gal3) belongs to a superfamily of carbohydrate-binding proteins (lectins), and it is characterized to bind with higher specificity to β-galactoside containing oligosaccharides. Gal3 is constituted by three domains: a short NH_2-terminal domain, a proline-rich collagen-α-like domain, and $COOH$-terminal carbohydrate-recognition domain [13].Gal3 is a pleiotropic protein that mediates processes like cell adhesion, proliferation, death, migration, survival, angiogenesis and metastasis in several tumors. Gal3 plays different functions, depending on its subcellular location (cell surface, cytoplasm, nucleus, endosomal compartment and mitochondria) and type of tumor [50, 51].

The silencing of the expression of a gene is done through interfering RNA (RNAi). In essence this stage can be obtained with the use of small interfering RNAs (siRNA) or by cloning of the cDNA reference in shRNA (short hairpin RNA). Synthetic siRNAs have short half-lives and, consequently, inhibition is restricted to short periods. The main advantages of vector cloning are: the higher molecular stability of DNA; the possibility of amplification in bacteria; permanent silencing of the target gene; the production of a large number of silenced cells and maintenance of the phenotype altered for long periods of time [52]. RNAi systems use lentivirus for a better efficiency in shRNA delivery of interest in the target cell. Lentiviruses are originally derived from HIV-1 (Human Immunodeficiency Virus-1) which, however, are unable to replicate. Once inside the cell, viral RNA undergoes reverse transcription and is transported to the nucleus [53] where it is finally integrated into the genome [54].

For the production of these lentiviruses, the expression plasmid encoding the shRNA of interest is transfected together with two other helper plasmids that express in trans the structural proteins and those necessary for the transcription step. With the aid of the cellular machinery, lentiviruses produce viral particles containing the shRNA, which accumulate in the culture medium supernatant. This supernatant can then be used for the transduction of the cells of interest, i.e., the target cells for gene silencing.

2 Materials and Methods

2.1 Cell cultures

The studies performed within the frame of the presented dissertation were carried out using keratenocytes cells and human melanoma cell lines. All cell lines have been cultured for many years at the "Instituto do Câncer do Estado de São Paulo Octavio Frias de Oliveira" (ICESP) in São Paulo, Brazil. All the cells were cultivated in the same culture medium, in order to reduce factors that could contribute to mechanical differences among them. Cultures were carried out in glass coverslips of 30 mm of diameter and with a density of 10^4 $cell/well$. HaCaT cells and WM1366 melanoma cells were cultured in DMEM (Invitrogen) medium supplemented with 10% fetal bovine serum (FBS from Gibco), respectively. All cultured cells were maintained in a humidified incubator with 5% CO_2 at 37°C. The culture time was set to 144 hours.

2.1.1 Generation of lentiviral particles and viral Transduction

Lentiviral particles, containing the shGAL3 (Openbiosystens, Lafayette, USA) pLKO1 constructs containing the short hairpin (shRNA) encoding sequence against the galectin-3 or shSCRB (Openbiosystens) pLKO1 transcripts containing the coding sequence for shRNA against unrelated sequence used as a negative control (scramble, SCRB) (OpenBiosystems), was generated by transfection of HEK293FT cells. In the transfection routines, mixtures containing the shGAL3 or shSCRB pLKO1 constructs (5ug/35mm dish) was used together with the constructs pLP1, pLP2 (packer plamids, both 2.5ug/5mm dish) and pLP / VSVG (5ug)/35mm plate) of the Virapower lenticular particle production kit (Invitrogen). After 24 hours of transfection, the culture medium containing the viral particles was collected and inactivated in accordance with level two biosafety.

The culture medium containing lentiviral particles obtained as described above was immediately centrifuged for removal of cell debris and supplemented with 6 $\mu g/ml$ hexadimethrin bromide (Polybrene®, Sigma). The mixture was transferred to culture of SK-Mel-37, SK-Mel 29 and WM1366 cells having confluence of the culture area between

$80 - 90\%$. The cells were incubated for 24 h. After this time the culture medium was replenished with fresh medium in the presence of 1 $\mu g/ml$ puromycin (Invitrogen). In parallel, the same procedure will be performed with a culture of non-transduced WM1366 cells. Cultures will be maintained under selective pressure, with periodic replacement of the culture medium until the death of the entire population of non-transduced cells.

2.2 Sample preparation for AFM measurements

For elasticity measurements using atomic force microscopy, cells were fixed with 4% paraformaldehyde for 15 min in PBS and were preserved in PBS with 0.01% azide at $4°C$. Prior to AFM measurements, glass coverslips with cells were immersed into the AFM fluid cell setup, filled with corresponding PBS and placed on the AFM piezo-scanner.

2.3 Atomic force microscopy

Atomic force microscopy (AFM) was created by G. Binnig, C. F. Quate, and Ch. Gerbe five years later of the scanning tunneling microscopy (STM) invention [55]. Its invention was motivated by the necessity of a technique capable of measuring non conductive samples, then AFM was applied to biological systems quickly. The technique has high spatial resolution, allows to precise control of the applied forces and its principle of operation is not affected by the environment around the probe, therefore it can be operated in liquid conditions, i. e. close to physiological conditions. At the begining, AFM was only applied to obtain topographical information of biological systems. The technique was adapted to the study of elastic properties of the samples over time.

2.3.1 Fundamentals of the technique

The atomic force microscopy is a technique based on the measurement of the interaction force between the sample surface and the probe, which consist in a sharp tip mounted at the end of an elastic cantilever. The interaction between the sample surface and the probe results in bending of the cantilever. Measuring the cantilever deflection, it is possible to evaluate the tip-surface interaction force, this information is used to form an image.

For the measurement the cantilever deflection an optical system is used. In such system, a laser beam is focused at the free end of the cantilever just above a probe tip. The reflected beam is guided towards the center of the photodiode, a position-sensitive detector (see Figure 2.1). Whenever the interaction force between the tip and the sample surface changes, the cantilever will bend, and thus the position of the laser spot on the photodiode changes. The measured signals are in volts and it is transmitted to the feedback system, which is used to retract or extend the piezoelectric scanner, where the sample is placed and which provides three-dimensional sample positioning with high resolution. On the other hand, the measurements of the mechanical properties require the AFM working in

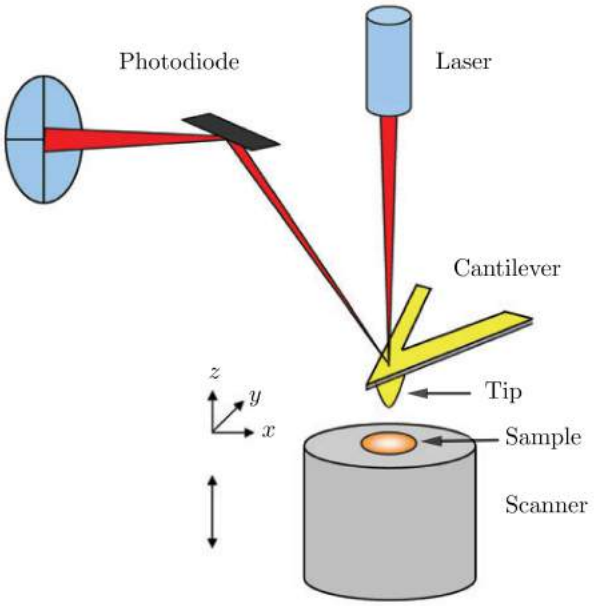

Figure 2.1: AFM basic configuration scheme. The sample is mounted on the piezoelectric scanner which ensures three-dimensional positioning with high resolution, and the force between the tip and the surface is monitored by measurement the cantilever deflection using an optical system constituted by a laser and photodiode, adapted from [31]

the so-called *force spectroscopy* mode where X and Y scanning is disabled. In this mode, the cantilever approaches the sample in z direction at a given spatial position, contacts it, and when it reaches the maximum deflection value and then withdrawn. The recorded cantilever deflection contains the information about the sample stiffness and also about any adhesive interaction occurring between the probing tip and the investigated surface [56, 15].

2.3.2 Operating modes

In order to understand how AFM modes work, it is necessary to describe the interaction when the tip approaches the sample surface. Lennard-Jones potential is suitable to describe the interaction of a surface atom and the tip, since the force involved is the van der Waals type. In Figure 2.2 a schematic force-distance curves is shown. Since the force can be attractive ($F < 0$) or repulsive ($F > 0$), there are different regimes that have to be considered. When the tip is far away from the sample surface, the cantilever does not have deflection because the interactive force is negligible. When the tip approaches the surface, the tip experiences an attractive force. Once the gradient of the attractive force equals the cantilever sprig constant, the tip jumps into contact with the surface. According to Newton's third law, the sample also exerts the same force on the tip. Thus, the tip is now getting into the repulsive force regime. The force will increase until a certain deflection value. In the repulsive regime, the contact mode is carried out, where the tip of the probe is always touching the sample (typical force values 10^{-6} to 10^{-9} N). In non-contact mode, the tip oscillates and it is kept a few tens of nanometers from the

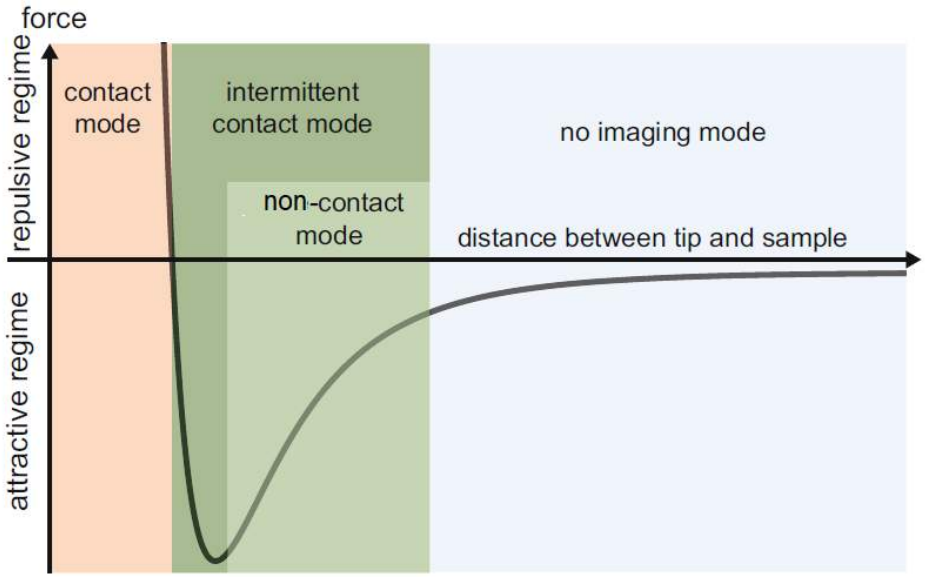

Figure 2.2: Schematic illustration of force-distance curve to describe the interaction between the cantilever tip (probe) and the sample surface labeling the different operation modes.[56]

sample surface, thus operating in the attractive regime (typical force value $10^{-12}\ N$). And finally, in the tapping or intermittent mode, the cantilever oscillates between the regions shown in Figure 2.2. Due to the fact that all the AFM images present in this work were obtained by the AFM contact mode, more detailed description of this operating mode will be given next.

AFM-contact mode

In this operating mode the tip at the end of the cantilever is kept in contact to the sample surface during the experiment. During the scanning, the tip passing through points of different heights, generating variations in the cantilever deflection. In this case, the cantilever is modeled as a spring, and its deflection is proportional to the tip-sample force. If the stiffness of the cantilever spring (spring constant) is known, the force between tip and sample can be determined by measuring the bending of the cantilever. The force is given by Hooke's law:

$$F = -kz, \tag{2.1}$$

where F is the force (typically between nN and μN), k is the spring constant, which can be from $0,01N/m$ to $1,00N/m$, and z is the distance the cantilever is bent relative to its equilibrium position. The deflection of the cantilever is measured using a laser beam reflected from the back of the cantilever into a split photodiode as shown in Figure 2.1. Operationally, the image can be formed in two ways: (1) *constant force mode* (the most used operating mode), where the deflection of the cantilever is maintained constant during the sweep by moving the sample vertically, using feedback mechanisms together to the piezo scanner, at each point of the sample surface. The correction in the vertical position with the sweep in XY allows to obtain a topographic image of the sample surface; and (2) *constant height mode*, where the cantilever deflection is measured, point to point, without

making corrections in the height (with no feedback active). This mode is mainly used for real time image recording of surfaces in formation, due to its high scanning speed.

As well as the cantilever is modeled like an harmonic oscillator with elastic constant k, the sample surface also is considered like a set of coupled oscillators with effective elastic constant of interatomic coupling k_{at}. With the purpose that during the contact the cantilever is deformed instead of the sample surface, the probe should be chosen such that $k << k_{at}$. It is important to point that in addition to the van der Waals force, a thin water layer usually present at the sample surface exerts an attractive capillarity force on the tip. This force is about 10^{-8} N and constant during the scanning for steady-state ambient conditions. In cell biology, the contact mode has been largely used to topographic image, to explore membranes of living cells, cytoskeletal structures, and lamellipodia of migrating cells[58, 59, 60, 61].

2.4 Force Spectroscopy

Force spectroscopy is a technique to measure a local force acting on the tip, exerted by a sample with spatial resolution in the nanometre scale. While AFM imaging is performed by scanning the sample (or tip) in the XY-direction, force spectroscopy is done by approaching and retracting the tip (or sample) in the Z-direction. The elastic properties of living and fixed cells are determined by analyzing force versus indentation curves.

2.4.1 Force curves

There are two force curves: the one recorded during approaching of the tip to the sample surface (an approach curve, the blue one in the Figure) and the other one collected during opposite motion (a retract curve, the red one in Figure 2.3). The shape of the force curve depends of the physical and chemical properties of the two interacting surfaces.

In Figure 2.3, a typical force curve, taken at the LFF, in steady-state ambient conditions is shown. On the horizontal axis of the graph the movement of the tip relative to the sample surface is presented. As the tip descends, the distance between the tip and the sample decreases, and the deflection of the cantilever is plotted on the vertical axis.

In the vicinity of point **A** the cantilever is far from the surface and its deflection should be zero since there is no detectable interaction force. The measured deflection reflects the noise present in the AFM system. The cantilever oscillates around its free position due to thermal vibrations. During the approach, if both the tip and the surface are charged with the same sign, at close distances, prior to the contact, the cantilever can be repulsed from the surface. This is represented by the slight raise in the base line. Then, the presence of attractive forces between the tip and a surface is reflected by a jump–in (point **B**), i.e. the cantilever is suddenly attracted. At this moment, the gradient of the attractive force is larger than the cantilever spring constant. When the tip is in contact with the sample surface, the electron clouds of atoms, of both the tip and the sample, are

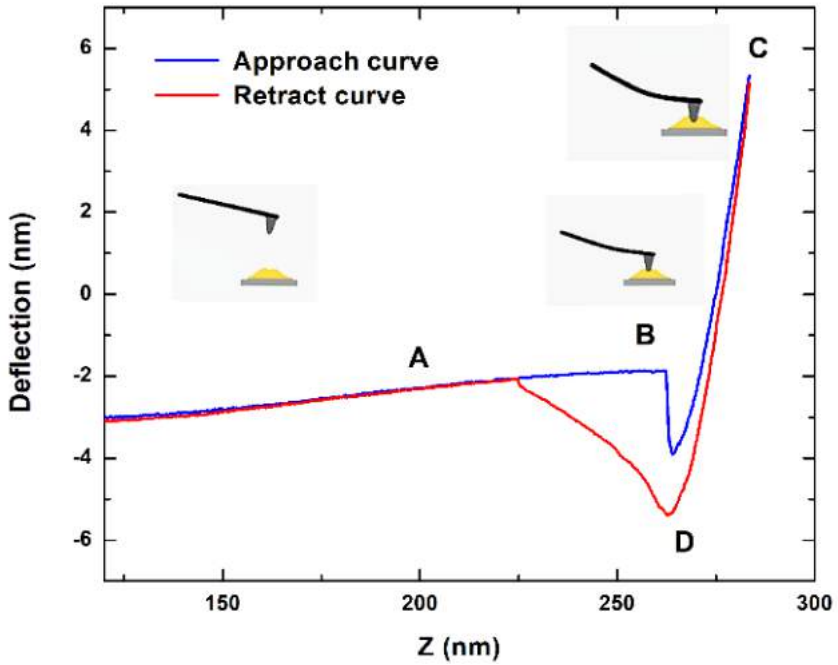

Figure 2.3: Force curve of a capillary fiber taken in the LFF at ambient conditions, using the Bruker Multimode V SPM microscope and a piramidal tip with spring constant of 25 N/m. In the plot can be seem a negative peak in the retraction curve. This indicates adhesion phenomena between the tip and the sample, resulting in the bending of the cantilever in the opposite direction than that when it is pressed against the sample. In addition, the retraction curve is below the approach curve, i.e. the force between the tip and the sample produced for the same deformation is lower, which indicates viscous (dissipative) behaviour of the sample, implying that the applied deformation is partially irreversible, or occurs at much longer time than the duration of the measurement.

overlapping and repulsing. The further approach results in the cantilever bending (up to the certain maximum value, point **C**), which profile depends on the material properties of the investigated sample (linear or not). During separation of the two surfaces, the interacting repulsive force decreases [15].

Finally, during retraction the tip does not separate from the surface exactly at the same point where it started to touch the surface. Forces that are responsible for such behavior arise from adhesive properties of investigated surfaces. In further retraction, when the elastic force of the cantilever exceeds the gradient of the adhesive force, the tip is rapidly separated from the surface. Point **D** corresponds to the maximum value of this force (the so-called pull-off force). The adhesion forces are associated to the capillary bridge between the tip and the sample, and depend if measurements are made in air or in liquid. In air, samples usually have several nanometers of water molecules adsorbed in their surface. This water layer forms the bridge between the tip and the sample, with a large force being required to overcome the surface tension and pull out the tip from the sample. In liquid conditions, the adhesion force not only depends of the interaction energies between tip and sample but also on the type of solution used [63, 32].

For hard substrates (non-deformable), such as a sapphire, the deflection increases linearly with the vertical movement and both curves are superposed unlike soft biological samples that are deformed when the cantilever is brought into contact.

The elasticity properties are determined from the contact region of the force curve. So, a high adhesion limits the information that can be obtained from a force curve. In order to reduce adhesion and capillarity forces, measurements in liquid medium are preferable. This is an advantage for biological systems that need to preserve their physiological environment during the experiment.

2.4.2 Determination of the elastic modulus

Elastic modulus can be obtained from the shape of the force-indentation curve. The deformation (indentation) of the sample, δ, at each point of the force curve is given by the difference between the vertical distance traveled by the cantilever, z, and the corresponding deflection d:

$$\delta = (z - z_0) - (d - d_0), \tag{2.2}$$

where d_0 is the zero deflection and z_0 is the z position at the contact point.

On hard samples, the point of contact z_0 is easily determined by the intersection of the two linear regimes (before and after contact with the sample surface). The same procedure presents more difficulties in the case of soft samples. In fact, when the tip touches a cell, the change in the deflection signal is not neat. Instead, the slope gradually increases and the point of contact results hidden in the noise and smoothed by tip-surface interactions. Additionally, because force curves on soft samples are, in general, not linear, the point of contact cannot be obtained from the simple intersection of two regimes, but rather needs to be fitted with appropriate models. This nonlinearity can be attributed to changes in contact geometry between the probe and the sample at increasing indentations. Accordingly, to describe the elastic behavior of a sample that undergoes deformation, models that take into account the tip shape are needed.

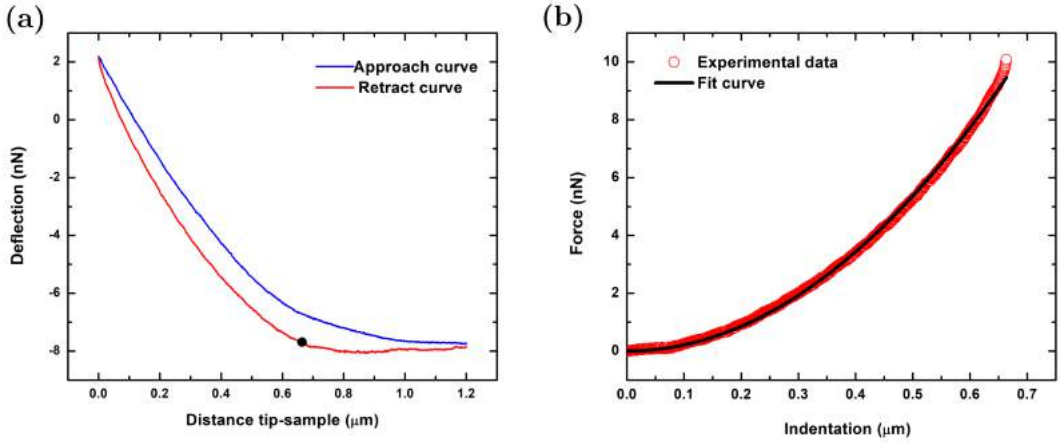

Figure 2.4: (a) Force curve acquired in the center of the HaCaT cell. The modulus of elasticity was determined from the retract curve. The point on this curve corresponds to the contact point calculated by the AtomicJ software. (b) Force-indentation curve together with its fitting. Using the equation 2.4 it was determined the elastic modulus.

Several different mechanical models have been developed for the analysis of force-indentation curves. The most common model applied in biological samples is the classical

Hertz model [64], which describes the indentation of a sphere into a homogeneous, soft, and semi-infinite elastic material. At this point, it is known that a cell cannot be treated as a thick and elastic half-space due to its internal structure, which is composed of materials characterized by distinct mechanical properties. Despite the ongoing development in modelling of mechanical properties of single cells, the Hertz contact theory is still dominant in the analysis of elasticity of single cells. The extension of this model for the conical-shaped tip and the four-sided pyramidal-shaped tip like indenter were given by Sneddon [65] and Bilodeau [66], respectively.

In this work four-sided pyramidal tips were used because this kind of tip is associated to a cantilever with low spring constant and has been used with good results in the differentiation of normal cells and cancer cells. So, for an ideal four-sided pyramid tip, the equation of force (F) as a function of indentation depth (δ) is defined as:

$$F = \frac{1}{\sqrt{2}} \frac{E \tan\theta}{(1-\nu^2)} \delta^2, \tag{2.3}$$

where, E is the sample Young's modulus, θ is the opening angle of the tip and ν is the Poisson ratio, which represents the compressibility of sample material. The Poisson ratio for cells is unknown and difficult to determine, therefore in all calculations its value needs to be assumed. Very often this value is simply set to 0.5, since cells can be treated as soft incompressible material [67]. The final expression used to determine E from force curve is:

$$d = d_0 + \frac{1}{\sqrt{2}k} \frac{E \tan\theta}{(1-\nu^2)} [(z-d) - (z_0 - d_0)]^2. \tag{2.4}$$

In order to analyse the force curves acquired, *Atomic J software*[68] was used. The software was configured to determine the contact point through successive search, i.e., every point of the curve is assumed a trial contact point. A polynomial is fitted to the pre-contact part of the curve, and the the appropriate contact model is fitted to the force-indentation data. The corresponding sums of squares are recorded. The point that gives the lowest total sum of squares is accepted as contact point. In Figure 2.4(a) is presented a force curve taken in the central region of a HaCaT cell. The contact point was determined from the retract curve. Then, the force-indentation curve was plotted and fitted using the Hertz model (see figure 2.4(b)).

The modulus of elasticity can vary around 100 GPa for materials like sapphire, 100 MPa for polymers and 1 MPa for soft materials. In 1999 Radmacher [69] summarized the values of elastic modulus for some representative materials including living cells (see Table 3.2).

Table 2.1: Elastic modulus of various materials. Adapted from [69].

Material	Elastic modulus
Steel	200 GPa
Glass	70 GPa
Bone	70 GPa
Collagen	1 GPa
Protein crystal	0.2 to 1 GPa
Rubber	1.4 MPa
Living cells	1 to 100 kPa

2.5 Procedures and experimental features

2.5.1 AFM setup

The *Bruker Multimode 8 SPM (MM-SPM)* with NanoScope V controller and NanoScope Analysis software that was used to collect the AFM data presented in this dissertation is shown in Figure 2.5. The microscope is combined with an optical vision system, which consists of a camera mounted vertically over the head of the SPM to view both the sample and tip [72]. This system allows the control of the AFM tip position and selection of a specific cellular region on the sample. In addition, the MM-SPM is equipped with a fluid cell, which consists of a small glass assembly with a wire clip for holding an AFM probe, as shown in Figure 2.6. The glass surfaces provide a flat interface so that the AFM laser beam may pass into the fluid without being distorted by an unstable surface. The probe is mounted in a rectangular groove on the bottom of the fluid cell, and held in place by a gold-coated wire clip. A circular groove surrounds the probe is used to seat the O-ring, whose purpose is to confine the liquid over the scan area. Additionally, there are at least two fluid ports located on the front side of the fluid cell. These ports allow for the introduction and removal of fluid.

2.5.2 Imaging cells in liquid medium

The surface topographic measurements of different cell lines was carried out in AFM contact-mode under liquid environment. The fluid used was a Phosphate-buffered saline (PBS), which is a buffer solution commonly employed in biological research, since the osmolarity and ion concentration of the solution match those of the human body. V-shape silicon nitrade cantilevers with four-side pyramidal tip and half-opening angle of 35° were used as a probe [DNP-10 (Bruker) characterized by nominal spring constants of 0.12 N/m, microlevel type B]. In addition, for the WM1366 shGal3 cell line the surface of the cantilever was modified by sulfur hexafluoride (SF_6) plasma treatment [77], with the aim of making the probe surface inert and thus prevent that the melanin expressed by cells adhere to the cantilever. Before measurements, the sensitivity of the optical system was calibrated by taking a single force curve on sapphire surface using the method that

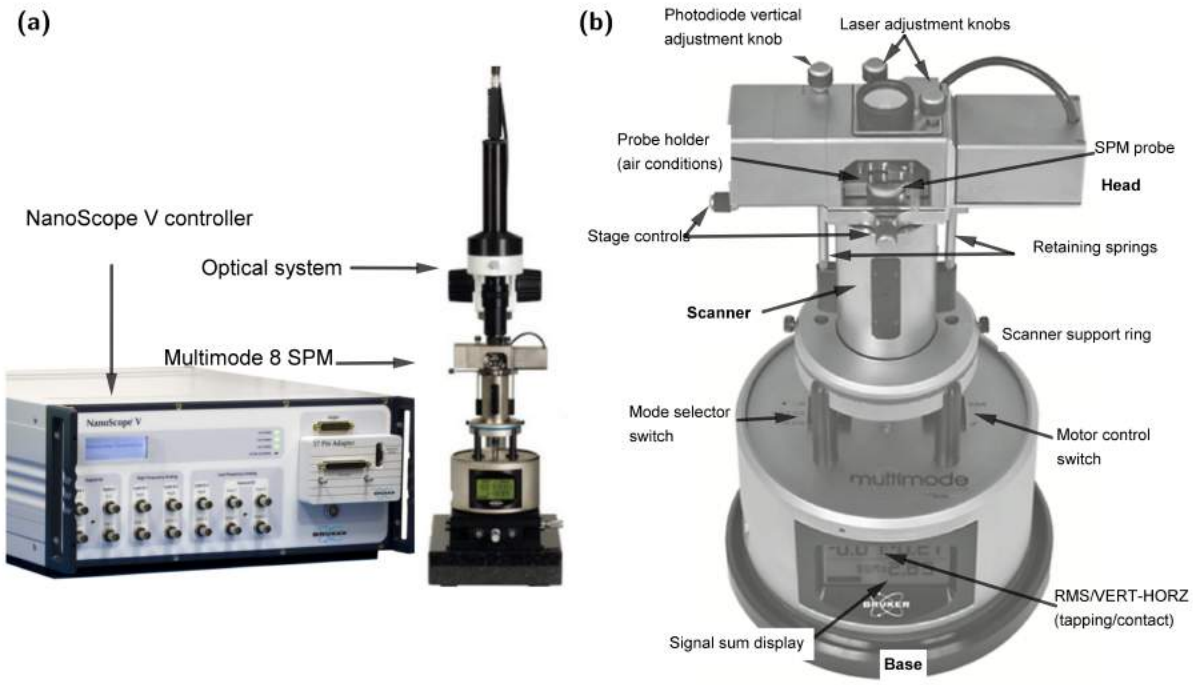

Figure 2.5: (a) Image of Bruker Multimode 8 SPM coupled to Optical Viewing System (OMV) and the NanoScope V controller, (b) different components of the SPM operating in air conditions. Adapted from [72].

will be described in Section 2.5.3. The cantilever spring constant was determined by the thermal tune method (also see Section 2.5.3).

AFM images were acquired following the steps:

1. The cells were washed three times with PBS.
2. The coverslip with the fixed cells immersed in PBS was mounted on the aluminum holder and fixed by magnets to the AFM piezoelectric scanner.
3. The fluid cell was mounted on the AFM head and filled with PBS to form the drop that covers the cantilever and the sample.
4. An optical image was collected to find relative positions of a cell to be measured and the tip (see Figure 2.7).
5. Images of surface topography were recorded.

2.5.3 Individual force curve

The elastic modulus of each cell line was determined from AFM force curves. In addition to the intrinsic mechanical response of the cell, certain parameters defined during the experiment influence the final shape of the curve, as discussed in chapter one. In order to acquire the most comparable data possible, after doing some tests, the same parameters were defined for all cell lines studied. The maximum indentation force is controlled by

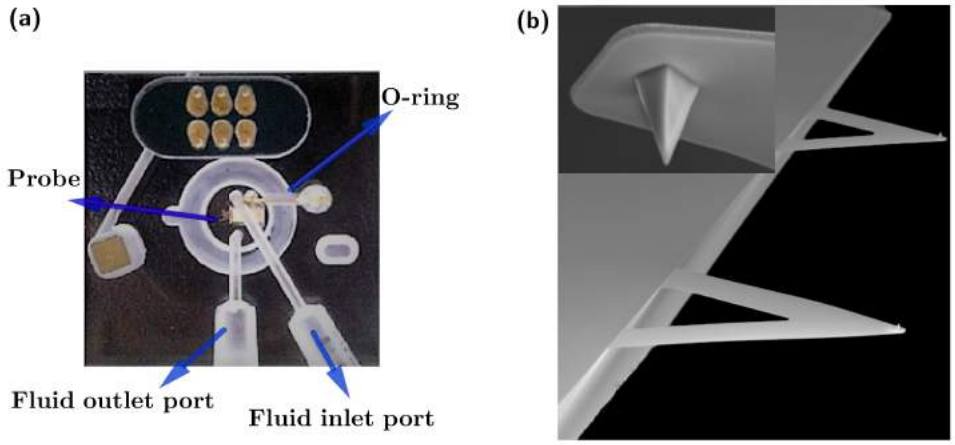

Figure 2.6: (a) Fluid cell model *MTFML* made by Bruker Instruments. For this model the probe, cantilever, and sample are completely immersed in the liquid. Adapted from [73].(b) Scanning electron microscopy image of V-shape silicon nitrade cantilevers with four-side pyramidal tip, model DNP-10 made by Bruker Instruments. The nominal cantilever length is 200 μm and the tip height is 8.0 μm. Adapted from https://www.brukerafmprobes.com

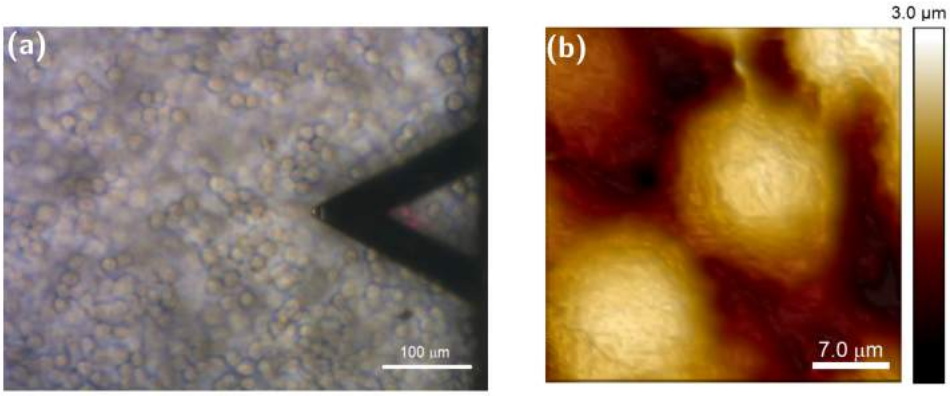

Figure 2.7: (a) Image acquired with the optical microscope coupled to the AFM, in which the cantilever and the sample can be observed, focus is on the sample. (b) Image of AFM obtained in contact mode and using the PBS buffer solution of HaCaT cells.

the trigger algorithm, which is associated with the maximum deflection of the cantilever during the indentation process. This parameter was established as 10 nN for all data. Similarly, the approach and retraction speed of the cantilever was selected within the range of 2 $\mu m/s$ to 3 $\mu m/s$, while the ramp size was 1200 nm. The protocol followed during the acquisition of force curves is shown below:

1. **Calibrate the deflection sensitivity.** In an AFM force spectroscopy experiment, it is essential to know exactly the deflection of the cantilever in nanometers. Therefore, prior to the measurements on the sample, the microscope must be calibrated (more specifically, calibrate the signal emitted by the photodiode) so that it converts the deflection of the cantilever from volts to nanometers (fundamental data to determine the elastic constant of the sample).

   The calibration procedure consists of recording a force curve on a stiff surface.

Some authors suggest to use an uncovered region of the coverslip that contains the adhered cells [7, 71]. However, it is arguable because, not necessarily, this region is intact and has not been modified as a result of the presence of the cells immersed in its extracellular matrix extending over the glass. Therefore, for this research, a sapphire surface was used. A typical calibration force curve is shown in Figure 2.8. Because the sapphire can be taken as a totally stiff material, the cantilever deflection registered after the probing tip touches the surface is linear, since deformation caused by the AFM tip does not occur. Sensitivity is determined as an inverse value of the slope of the force curve (in Figure 2.8 it corresponds to the region limited by the dashed lines) obtained from the linear fit to the region which the cantilever is in contact with this hard sample surface[72].

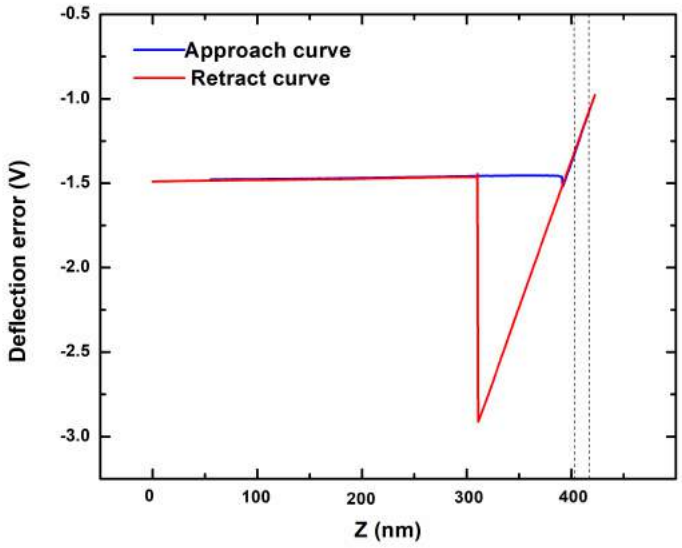

Figure 2.8: Force curve taken in air environment at the sapphire sample surface. The Deflection Sensitivity allows conversion from the raw photodiode signal (in V) to deflection of the cantilever (in nm), and its value reflects the properties of the optical system used for the cantilever deflection.

2. **Determination of spring constant.** As mentioned before, estimates of cellular elastic modulus are obtained by relating the force applied to the sample with the deformation caused on it. Accordingly, an optimal force measurement should display a large cantilever deformation, and also a marked degree of sample indentation. This is achieved by using cantilevers whose stiffness matches that of the probed sample. Cantilever's elastic properties are defined by the material it was made, which can be silicon or silicon nitrate, and its geometry, i. e., length, width, thickness, and shape. So, the elastic properties of the cantilever are quantitatively described by the spring constants, in case of cells measurements, it is within the range of 0.01 to 0.6 N/m.

   Although the expected stiffness of the sample should serve as an initial guide for choosing the rigidity of the cantilever, some authors suggest using slightly more rigid cantilevers, since too soft cantilevers can remain attached to the sample during

the retract curve. Then, if the cantilever is not separated from the sample at the end of the ramp cycle, the next approach curve will not have a flat part region without contact. One way to solve this problem is to use long ramps, which move the cantilever away from the sample so that detachment occurs. However, this occurs at the expense of high values of tip velocity which can lead to hydrodynamic contributions of the liquid environment surrounding the cantilever. On the other hand, the appropriate selection of shape tip depends on the type of experiments to be carried out. In this work the mechanical properties of the cells are measured to differentiate normal cells from cancerous cells. For this propose the pyramidal tip is used due to the fact that the majority of the results that have been reported showing a distinction between these cells used tip with pyramidal geometry. It is important to say that no detrimental effects due to persistent probing of cells with a pyramidal tip were reported in literature [74, 75]. In addition, using these tips is possible to combine simultaneous high-resolution mapping of the cell topography with localized mechanical properties, using the same tip.

The spring constants may differ substantially from values quoted by the manufacturer, which means that one must determine spring constants experimentally to get accurate knowledge of the measured forces. Next, the method used to determine the spring constants of the tips used during the investigation is described. Hutter et al.[76] developed a method to determine the tip spring constant from the measurement of its thermal fluctuations. In this context, a cantilever can be approximate as a simple harmonic oscillator with one degree of freedom for small deflections. In this way, the harmonic oscillator in equilibrium with its surroundings will fluctuate in response to thermal noise. The Hamiltonian of such system is

$$H = \frac{p^2}{2m} + \frac{1}{2}m\omega_0 q^2, \tag{2.5}$$

where q is the displacement of the oscillator, p is its momentum, m is the oscillating mass, and ω_0 is the resonant angular frequency of the system. By the *equipartition theorem*, the average value of each quadratic term in the Hamiltonian is given by $k_B T/2$, where k_B is the Boltzmann's constant and T is the absolute temperature. Hence,

$$< \frac{1}{2}m\omega_0 q^2 >= \frac{1}{2}k_B T. \tag{2.6}$$

As ${\omega_0}^2 = k/m$ the force constant may be obtained from a measurement of the mean-square spring displacement as

$${\omega_0}^2 = \frac{k_B T}{< q^2 >}. \tag{2.7}$$

Therefore, measuring the *rms* fluctuations of a freely moving cantilever with a sampling frequency much higher than its resonant frequency, allows the determination of the spring constant. The data is examined in the frequency domain and the area below the peak is a measure of the power of the cantilever fluctuations. Since the integral of the power spectrum equals the mean square of the fluctuations in the time-series data, the estimate of the spring constant becomes

$$k = \frac{k_B T}{P}, \tag{2.8}$$

where P is the area of the power spectrum of the thermal fluctuations.
It is important to highlight that the thermal tune method can be used in liquid environment and is ideal for probes with spring constant less than approximately 5 N/m, which is the case in this research.

3. **Mounting the sample in the microscope.** The cells are washed three times with PBS. Then the coverslip is mounted on the aluminum support and fixed by magnets to the AFM piezoelectric scanner. Also, the fluid cell is mounted on the AFM head and filled with PBS to form the drop that covers the cantilever and the sample.

4. **Acquisition of an image in contact mode.** A topographic image of the cells must be taken, then the region in which will be determined modulus of elasticity is selected.

5. **Force curve acquisition.** Before recording the force curves, the following measurement parameters must be chosen: maximum indentation force (trigger), ramp size, and vertical ramping speed.

2.5.4 Force Maps

Due to the fact that the elastic response of the cell is highly inhomogeneous, which is caused by the heterogeneous cytoskeleton structure, taking a set of equally spaced force curves in a give scan size seems to be an interesting approach to obtain more information about the system. This is possible using *NanoScope Force Volume (FV)* option in the microscope, which combines force measurement with topographic imaging. This operation mode is usually obtained in contact mode and can be collected in physiological conditions.

Basically, FV mode generates force curves over a given area of the sample. Each force curve is taken at a certain x-y position of the sample, and the set of curves form a three-dimensional arrangement or volume of force. The z value at each point (x, y) in the force volume corresponds to the deflection of the cantilever in that spatial position. The force map is accompanied by a topographic image, which is acquired in each pixel when the tip reaches the surface of the sample.

In order to exemplify the measurement protocol in force volume and to expose the information that can be obtained, results reported by Wang et al. [79], who investigated the mechanical properties of human pulmonary artery endothelial cells, are shown in Figure 2.9. In *(a)* a cell is identified by AFM scanning (large scan size), where it is possible to visualize some morphological details of cells; then in *(b)* higher resolution deflection image, indicated with square in (a), is acquired. In this case the selected area contains part of the nuclear, cytoplasmic and peripheral regions. In *(c)* a force volume map generated by the AFM indentation with 32×32 force curves collected on $70 \times 70 \mu m^2$ area is shown, and in *(d)* the elastic modulus map generated by the force-indentation curves, fitting at each pixel, using the Hertzian contact mechanics model for spherical indenter is presented.

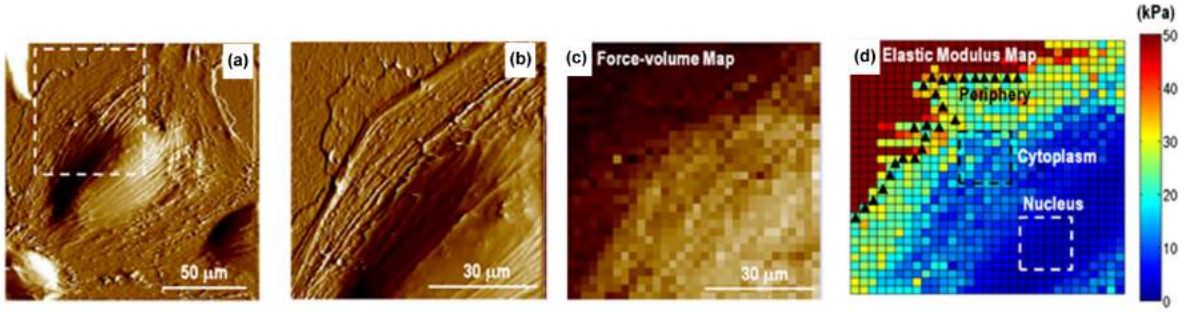

Figure 2.9: (a)Topographic image of a single human pulmonary artery endothelial cell. (b) Higher resolution image of the same cell in (a). (c) Force volume image generated by the AFM indentation, and (d) elastic modulus map obtained fitting each curve using the Hertzian contact mechanics model, showing soft cell compared to rigid substrate. The authors also identified the nucleus, cytoplasm and periphery regions in the elasticity map. Each curve was loading-unloading with roughly 1.5 $\mu m/s$ and the maximum force applied was 2 nN. Adapted from [79].

3

Results and discussion

3.1 Morphological analysis of the cells

The specific aim of the presented dissertation is to measurement cell mechanical characteristics that enable to differentiate between HaCaT cell line and WM1366 cell line, being the last one derived from the primary tumor in radial growth phase (RGP), i.e. not metastasis phase. As a first step, surface morphology was characterized by atomic force microscopy.

AFM topographic images were acquired in contact-mode under liquid environment (PBS). In order to minimize cellular damage, images were acquired with a scan rate between 0.40 Hz and 0.60 Hz and 96 points per line. These conditions increase the measurement time but then allow to obtain more reliable measurements of mechanical properties. Also, a low deflection set point was selected with the purpose of minimizing the lateral force exerted on the cell. It also avoided changes in the morphological conditions, particularly at the border cells, i. e., pericellular space (the thinnest cell regions).

Figure 3.1 shows the AFM morphological images for each cell line. Large scan size images of 100 μm × 100 μm for HaCaT keratinocytes cells (see Figure 3.1(a)) confirm co-confluences condition, such that it is not possible to acquire images of isolated cells. In order to observe details of the cell surface, smaller scan areas of $30\mu m \times 30\mu m$ were chosen (see Figures 3.1(b) and(c)). HaCaT keratinocytes cells present different formats, often showing a nucleus in the cell central region. Dense filamentous structures are appreciated at the cell borders, which are organized in parallel and connect adjacent keratinocytes, these structures are indicated in Figure 3.1 by white arrows. Also, in Figure 3.2(a) it is indicated the cellular protrude from the cell border, in regions that do not exhibit adjacent cells, i.e. intracellular structures are not observed. Unlike the keratenocyte cells, melanoma WM1366 cells show a more regular format and do not exhibit distinctive morphological features between shSCR and shGal3 cells (see Figure 3.1(d-i)). In addition, the cell and cell-cell junction regions do not present filamentous structures, as it was observed for HaCaT.

In general, the height of HaCaT cells is lower than WM1366 cells by about 1.0 to 2.0 μm,

as it is observed in the height profiles presented in the figure 3.2. Repeatedly, the height of the melanoma cells exceeded the vertical scan size range, which has a nominally value of 4.5 μm. These events made images with large scan size for the melanoma cells difficult to obtain, and so, numerous cells that were not correctly imaged were discarded for the characterization. This behavior may be due to the fact that neoplastic cells exhibit a tendency to overlap. Moreover, the melanoma cells silenced for the galectin-3 gene showed greater sensitivity to the scan rate, observing significant damage after successive scans, thus for these cells images were acquired using a scan rate of 0.3 Hz.

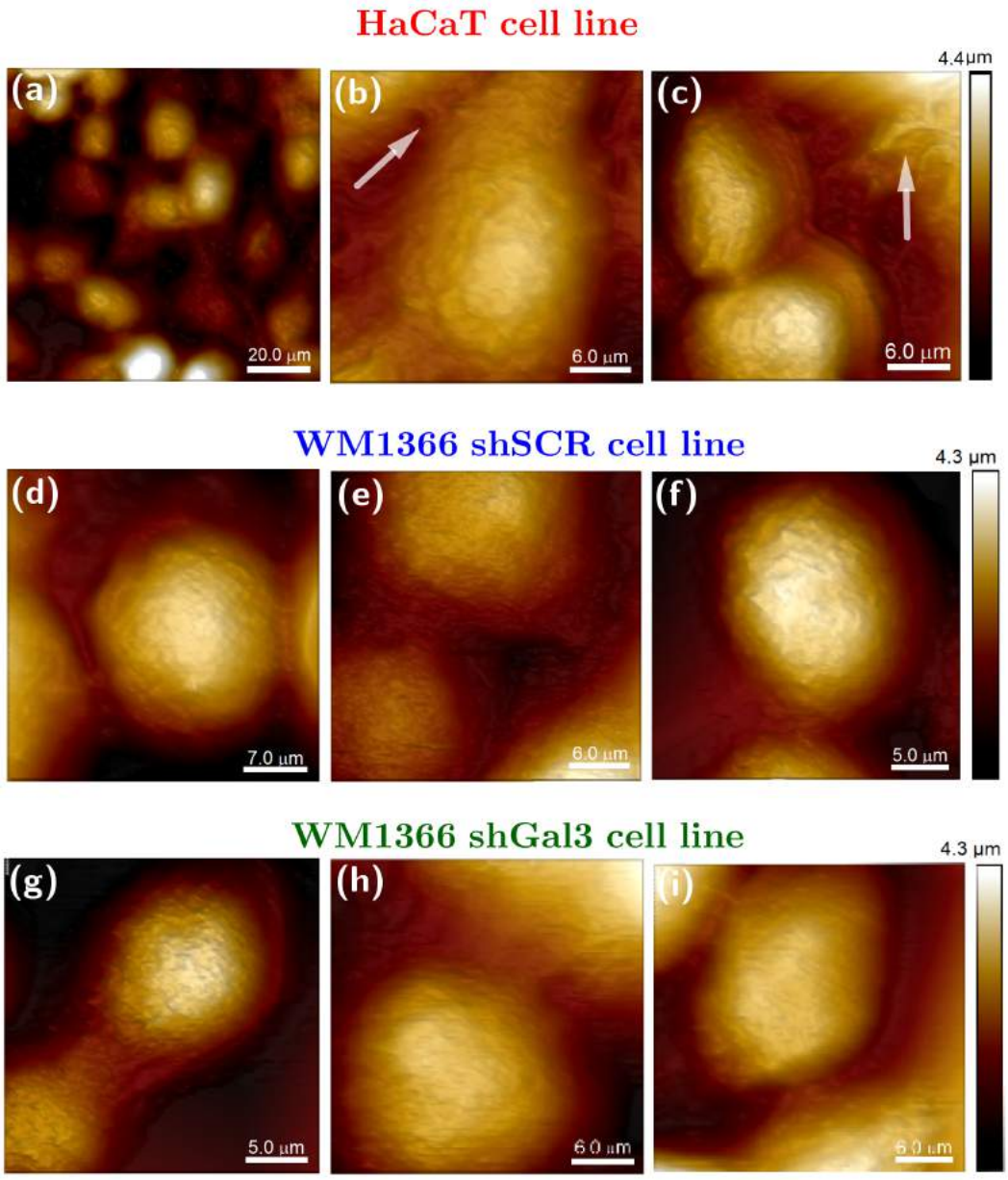

Figure 3.1: HaCaT keratinocytes cells topographic images (a) large scan size ($100\mu m \times 100\mu m$), that confirms co-confluence conditions, (b) and (c) high resolution images ($30\mu m \times 30\mu m$) that show intracellular structures in parallel organization that join adjacent keratinocytes. WM1366 shSCR topographic images (d), (e), (f) high resolution images (30 $\mu m \times 30$ μm). WM1366 shGal3 topographic images (g), (h), (i) high resolution images (30 $\mu m \times 30$ μm).

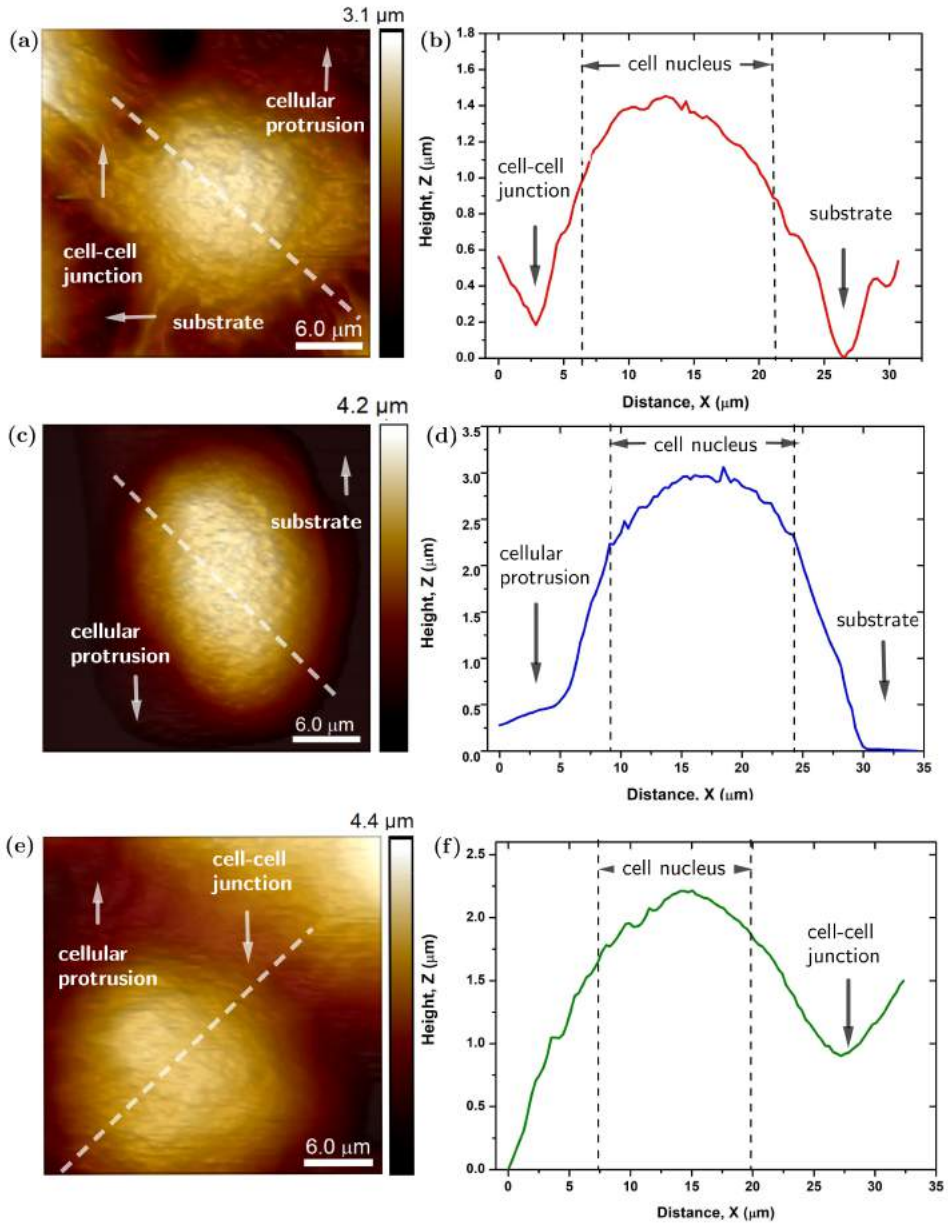

Figure 3.2: (a), (b) HaCaT keratinocyte cell topographic image, where is signaled the cell-cell junction and the cellular protrusion. Also, it is indicated the substrate, where the cell is adhered, and height profile of the cell respectively. (c),(d) WM1366 shSCR cell topographic image, in this case neighboring cells are not observed, and height profile of the cell respectively. (e),(f) WM1366 shGal3 cell topographic image, where is observed the cell-cell junction, whose shape differs significantly from the cell-cell junction of HaCaT cells, and height profile of the cell respectively.

3.2 Mechanical properties of the cells

The mechanical response of each cell line was investigated using two different approaches. In the ***first*** one individual force curves were taken in the central region of each cell. As a consequence of the complex cellular internal structure, during the indentation, the AFM

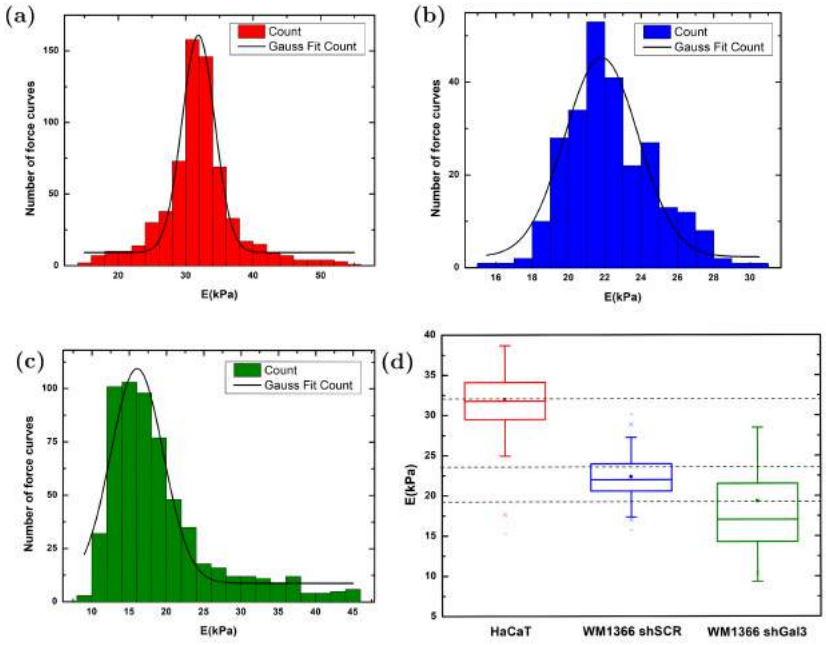

Figure 3.3: (a),(b),(c) Distribution of elastic modulus together with its Gaussian fitting obtained for indentations equal to 700 nm for HaCaT, WM1366 shSCR and WM1366 shGal3 respectitly. (d) Box-and-whisker plots of the elastic modulus distributions.

tip can find a variety of structures whose mechanical response can be different. Starting from glycocalix and the cell membrane, the AFM probe indents the cortex, formed by a network of actin filaments, and finally feels deeper parts of the cell, such as the cytosol and several organelles. Therefore, the indentation depth determines the cell regions that are probed [35]. For small indentation depth, the mechanical response will be dominated by the cell membrane tension and the surface layers of F-actin filaments, while deeper indentations provide information of different cellular organelles, such as the cell nucleus. In this research, force curves with large indentation depths were taken in the central region of the cell in order to probe cellular regions rich in all cytoskeleton elements (i.e. actin filaments, microtubules and intermediate filaments)[7]. In Figure 3.2(b,d,f) these regions are indicated. Due to the fact that the presence of the stiff glass substrate may result in an overestimation of the elastic modulus, indentations that do not exceed 20% of the cell height are recommended. Thus, force curves with indentations greater than 700 nm were discarded so as to avoid substrate effects in the measurements.

Table 3.1: Elastic modulus for each cell line studied.

Cell line	**E (kPa)**
HaCaT	31.9 ± 0.4
WM1366 shSCR	21.8 ± 0.5
WM1366 shGal3	16.1 ± 0.6

All the preset data were obtained from force curves acquired with trigger threshold set at 10 nN, ramp size in 1200 μm and approach and retract speed within the range of

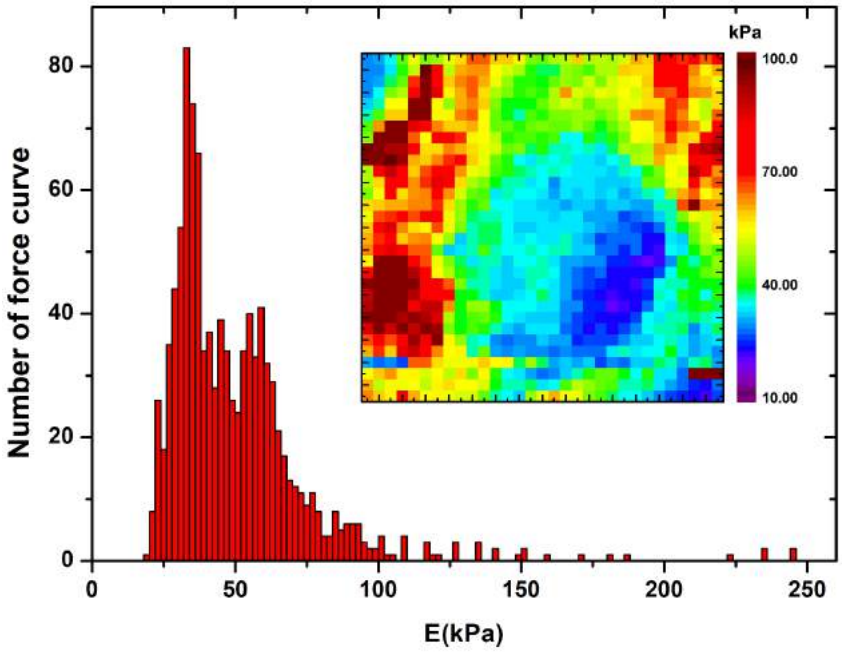

Figure 3.4: Elasticity map (32 × 32 pixels) and its histogram from the retract curves for a HaCaT cell.

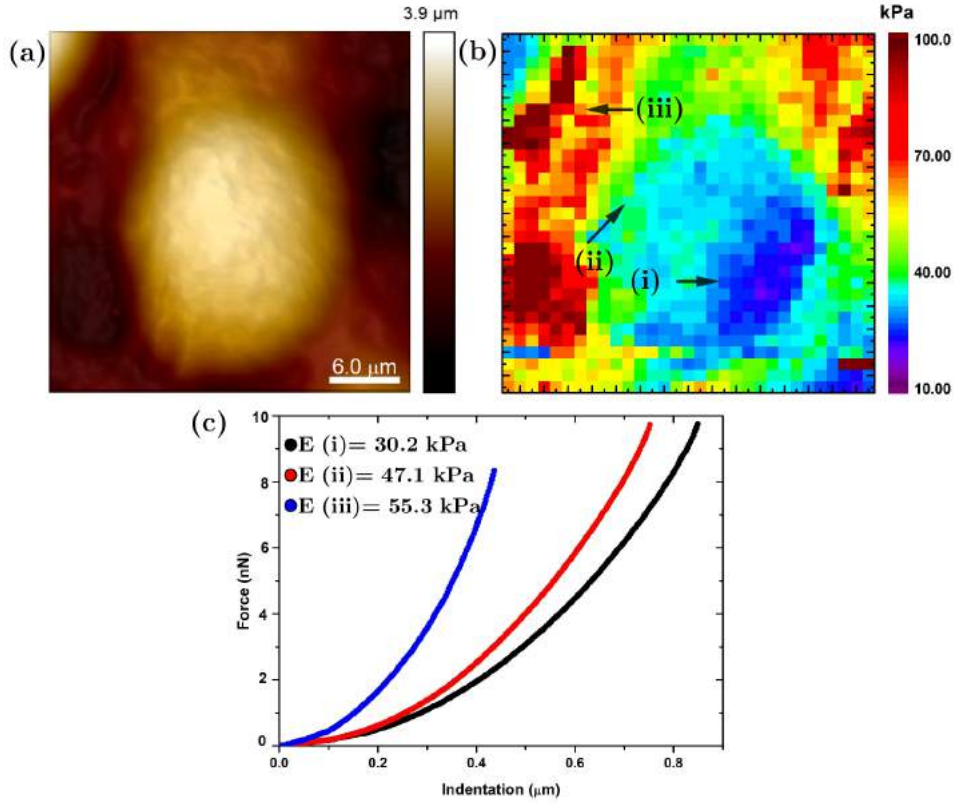

Figure 3.5: (a) Topographic image of HaCaT cell, (b) cell elasticity map, and (c) Force-indentation curves of some regions of the cell (i) cell center, (ii) cell border and (iii) substrate.

2 μm to 3 μm. In this work, 40 cells were tested and 600 force curves analyzed for each cell line. Force curves were analyzed with the Hertzian contact model for the pyramidal tip to determine the corresponding elastic modulus of individual cells. Figure 3.3 presents the distribution of elastic modulus of each cell line together with its Gaussian fitting obtained for indentations equal to 700 nm. In addition, Table 3.1 shows the mean values of the Gaussian fitting for each cell line. The error reported was calculated with a confidence level of 95%.

In order to compare the results obtained for each type of cell, box-and-whisker plots of the distributions are presented in Figure 3.3(d). The upper and lower whiskers represent the highest and lowest datum within 1.0 IQR (interquartile range). The median value of each distribution is also indicated by a horizontal line that goes through the box. The mean value is represented by a point inside the box, which is superimposed with the dotted line to ease the comparison of the distributions. The whiskers go from each quartile to the minimum or maximum.

The curves taken in the central melanoma cell exhibit smaller elastic modulus than keratinocytes (see Table 3.1), which is the result predicted by the literature [7]. The difference in cellular elasticity between the same cell line of melanoma, shSCR and shGal3, underline the fact that these cells can be distinguished for a large indentation depth, which represents general alterations in the organization of the cytoskeleton induced by the presence or absence of the galectin-3 protein.

Due to the fact that the cells have highly heterogeneous regions, an elasticity mapping would provide relevant information about these diverse cellular regions. This was the ***second*** approach followed in our work.

Elasticity maps with 32 $\times$ 32 force curves collected in a 32 $\times$ 32 μm^2 area were acquired for each cell line. The measurement parameters were kept constant throughout the experiment, and they are the same to those established for the acquisition of individual curves in the central region of the cell. In Figure 3.4 is presented de elasticity map and the histogram associated with the data map for HaCaT cell. The are represented on a scale of 10 up to 100 kPa, since it has been reported in the literature that cellular systems do not exceed a modulus of elasticity greater than 100 kPa. However, data associated with a greater modulus of elasticity were not eliminated in the histogram, because these data could be linked to the modification of the substrate (glass coverslip) as a consequence of the presence of the extracellular matrix. Figures 3.6 and 3.8 present elasticity maps together with the histograms associated with each map for WM1366 shSCR and WM1366 shGal3 cells.

Figure 3.5 shows the topographic image of the HaCaT cell next to the its elasticity map, which allows the correlation of cell morphology directly with its modulus of elasticity. From these images it is possible to identify, in the elasticity map, the cellular nucleus, which exhibits the smallest modulus of elasticity (as can be deduced from the scale that accompanies the map), the pericellular region, and deeper areas that we associate to the substrate in which the cells are adhered. Cell-cell junctions are also distinguishable in the elasticity map. To illustrate the variation of the slope of force-indentation curves with the cellular region probed, three curves from different map zone were extracted and their

respective values of E are also presented.

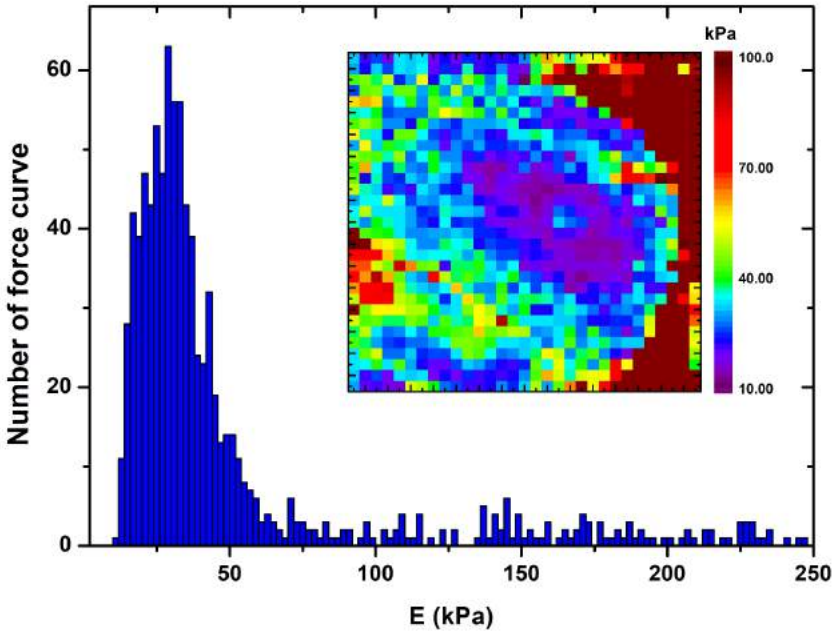

Figure 3.6: Elasticity map (32 × 32 pixels) and its histogram from the retract curves for a WM1366 shSCR cell.

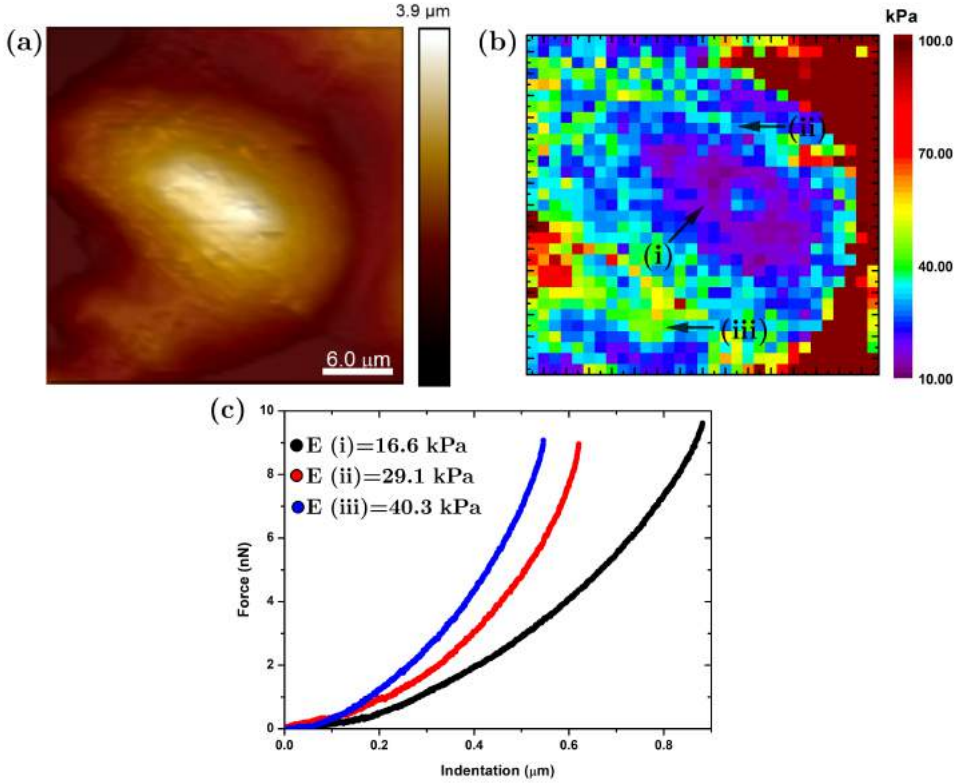

Figure 3.7: (a) Topographic image of WM1366 shSCR cell, (b) cell elasticity map, and (c) Force-indentation curves of some regions of the cell (i) cell center, (ii) and (iii) pericellular regions of cell.

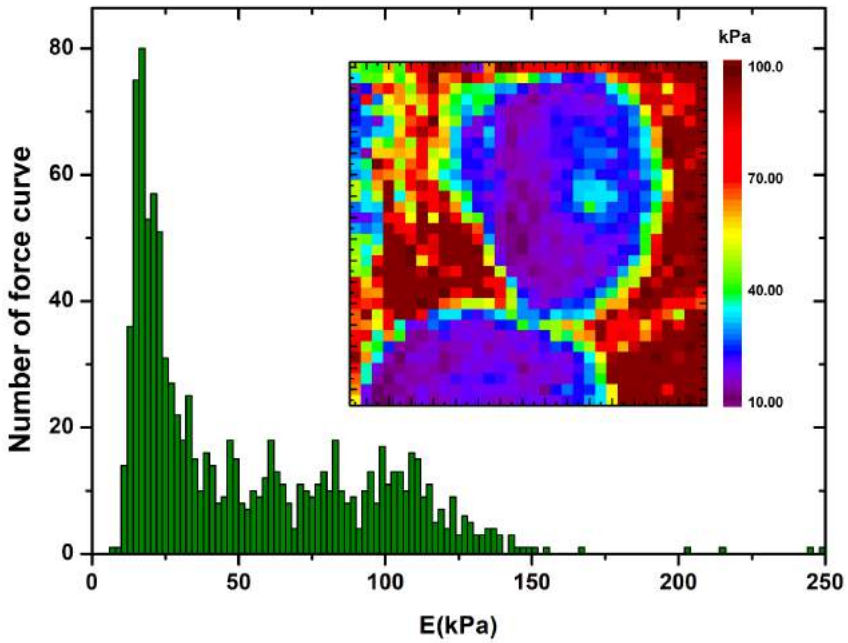

Figure 3.8: Elasticity map (32 × 32 pixels) and its histogram from the retract curves for a WM1366 shGal3 cell

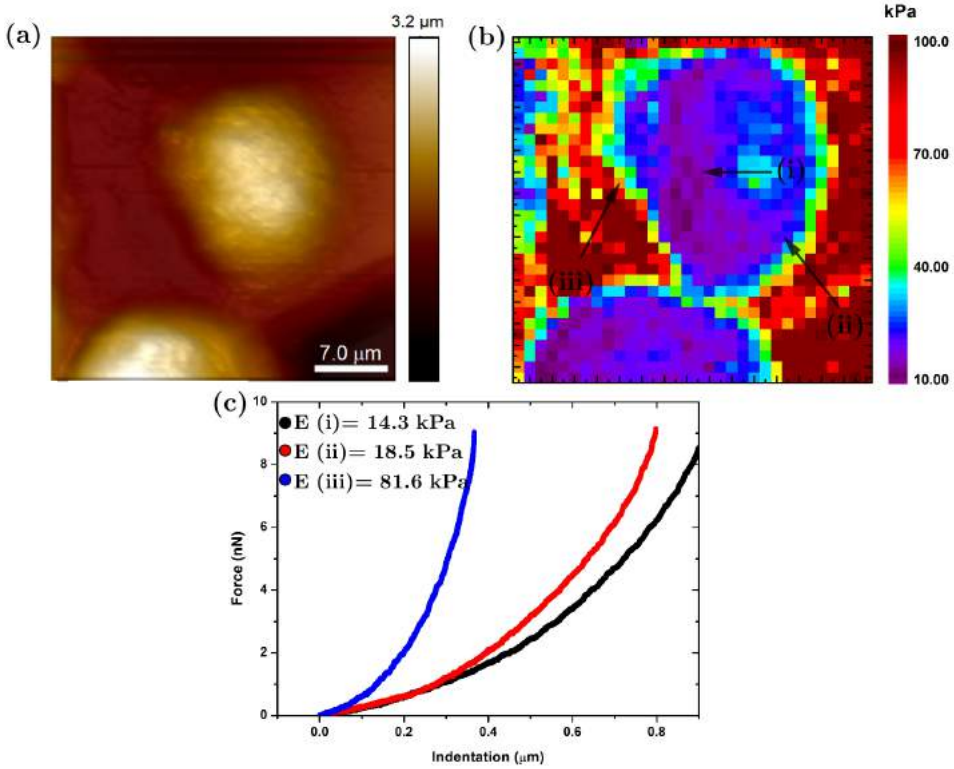

Figure 3.9: (a) Topographic image of WM1366 shGal3 cell (b) Cell elasticity map (c) Force-indentation curves of some regions of the cell (i) cell nucleus, (ii) pericellular regions of cell and (iii) substrate.

In the same way, elasticity maps of the melanoma cells were acquired, see Figure 3.6 and Figure 3.8 for WM1366 shSCR and shGal3 respectively. AFM topographic image next to the elasticity map is presented in Figure 3.7 for WM1366 shSCR cell, where the region of the cell nucleus is noted clearly. For WM1366 shGal3 cell, Figure 3.9 shows two cells visibly delimited. From the morphology image we deduce that there are no cell-cell junctions, as evidenced by the elasticity map.

In this manner, the information gotten from elasticity maps seems to be only qualitative and map histograms lack of physics meaning because the characteristics of the distributions depend on the size of the cell, the number of cells present and the area of the substrate within the map. These explain why the mean value of the distributions for the same cell lines and under the same experimental conditions are not in agreement. The elastic response of the cell is highly inhomogeneous, which is caused by the heterogeneous cytoskeleton structure underneath, added to that each cellular compartment has a particular elastic behavior. Therefore, using a similar protocol reported by Guo et al. [78], the cell was sliced into several different heights shown as a contour image in Figure 3.10. The contour line comprising the same color represents a height region within the same height section. After force indentations, curves of each height section were analyzed and represented in histograms, adjusted by the binomial distribution function. Table 3.2 shows the summary of the elastic modulus determined from this method for each height section.

In Figure 3.10 is presented the contour image for HaCaT cell in 3D, in which the height sections are indicated. The region R1 is the highest and corresponds to the center of the cell (cell nucleus). For this region, the modulus of elasticity found compatible with the value determined from individual force curves acquired in the HaCaT cell center (see Table 3.1). As shown in the figure 3.10, the elasticity distribution for R1 has the lowest standard deviation, which suggests that the cell region probed is relatively homogeneous. A similar behavior is observed in the R2 region. This is not the case of the R3 and R4 regions, which have been linked to the pericellular region, where a double peak elasticity distribution reveals more heterogeneous structure. The substrate was also probed and is represented by the R5 region. As already mentioned, the measurement parameters during the mapping of the elastic modulus are not readjusted, therefore it is important to take into account that the results obtained from these may have contributions from the substrate in the areas of lower height.

The contour image for WM1366 shSCR cell together with the elasticity distributions for each height interval are shown in Figure 3.11. The elasticity distributions of all regions were adjusted with a single peak. Due to the geometry of the mapped cell, the central region has a low number of force curves. For WM1366 shGal3 cell, Figure 3.12 shows the contour image. The distributions of the first three regions are narrow and their mean values remain closely. It is remarkable the wide difference in modulus of elasticity in the region more distant from the center of the cell between the melanoma cells that express Gal-3 and the melanoma cells in which the lectin was silenced (see histograms R1, R2 and R3 of Figures 3.11 and 3.12.)

To corroborate this final result, force curves were taken at the cellular periphery for melanoma cells. It was found that in this region melanoma cells that do not express

galectin-3 exhibit a modulus of elasticity of $69 \pm 4\ kPa$, unlike unmodified melanoma cells that have a modulus of elasticity of $30 \pm 2\ kPa$ (see Figure 3.13). These values indicate that the extracellular matrix of cells lacking galectin-3 has been modified.

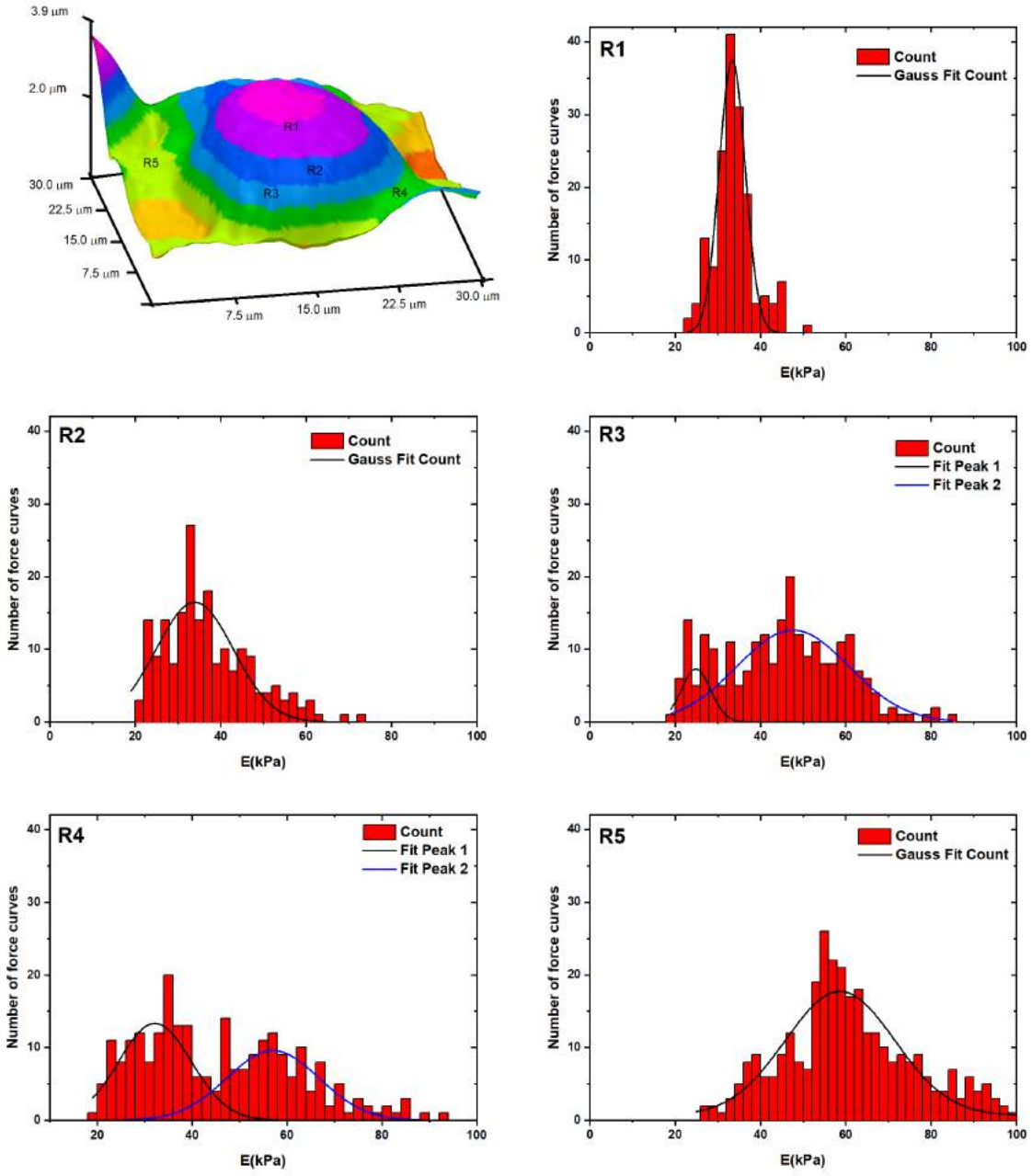

Figure 3.10: Contour image for HaCaT cell in 3D, for a better visualization of the cell the scale of the axis z is three times the scale of the axis x and y. The topographic image was sliced in five regions, clearly identified. The histograms associated with each of the regions together with their respective Gaussian settings are also displayed. The scales have been standardized for a correct comparison.

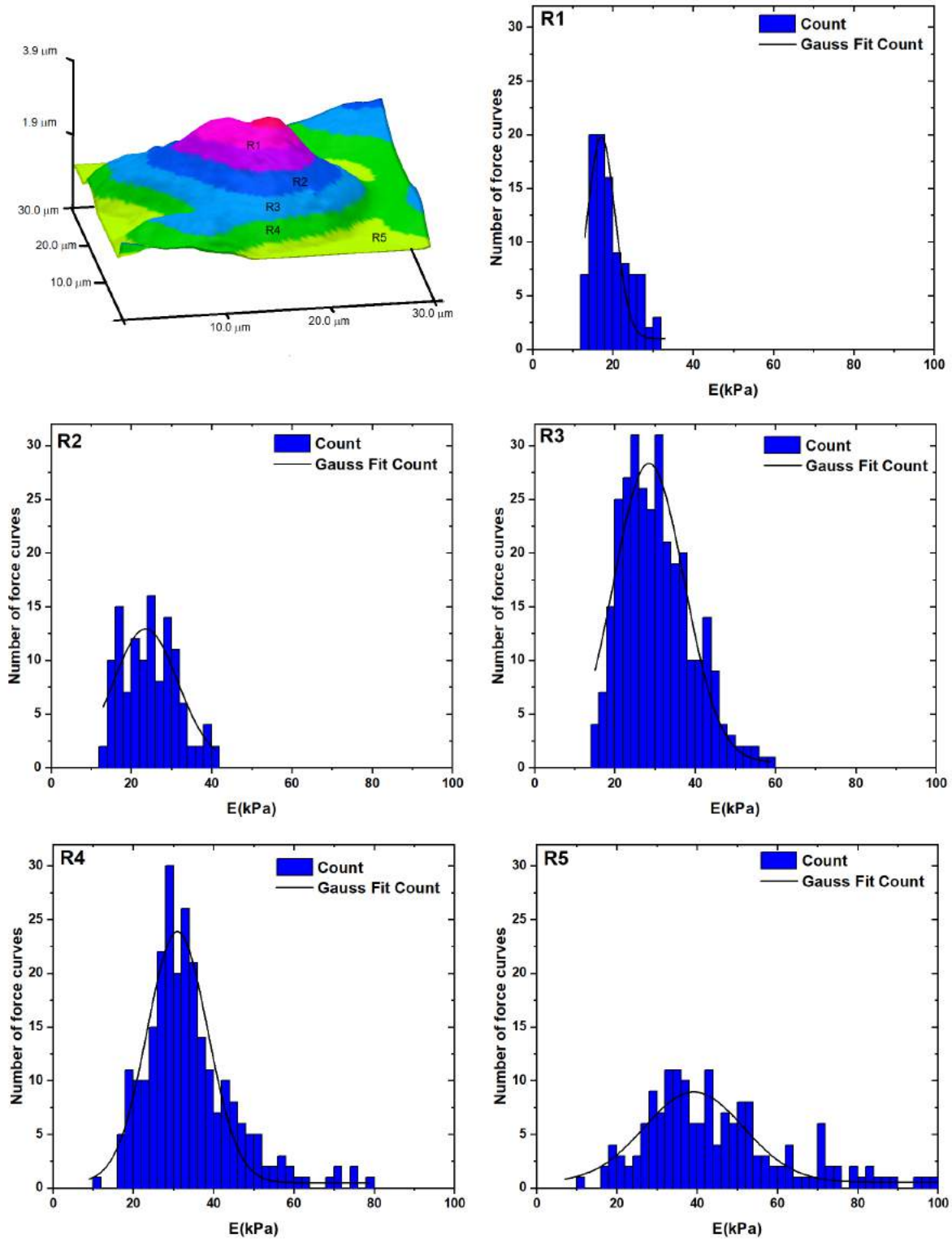

Figure 3.11: Contour image for WM1366 shSCR cell in 3D, for a better visualization of the cell the scale of the axis z is three times the scale of the axis x and y. The topographic image was sliced in five regions, clearly identified. The histograms associated with each of the regions together with their respective Gaussian settings are also displayed. The scales have been standardized for a correct comparison.

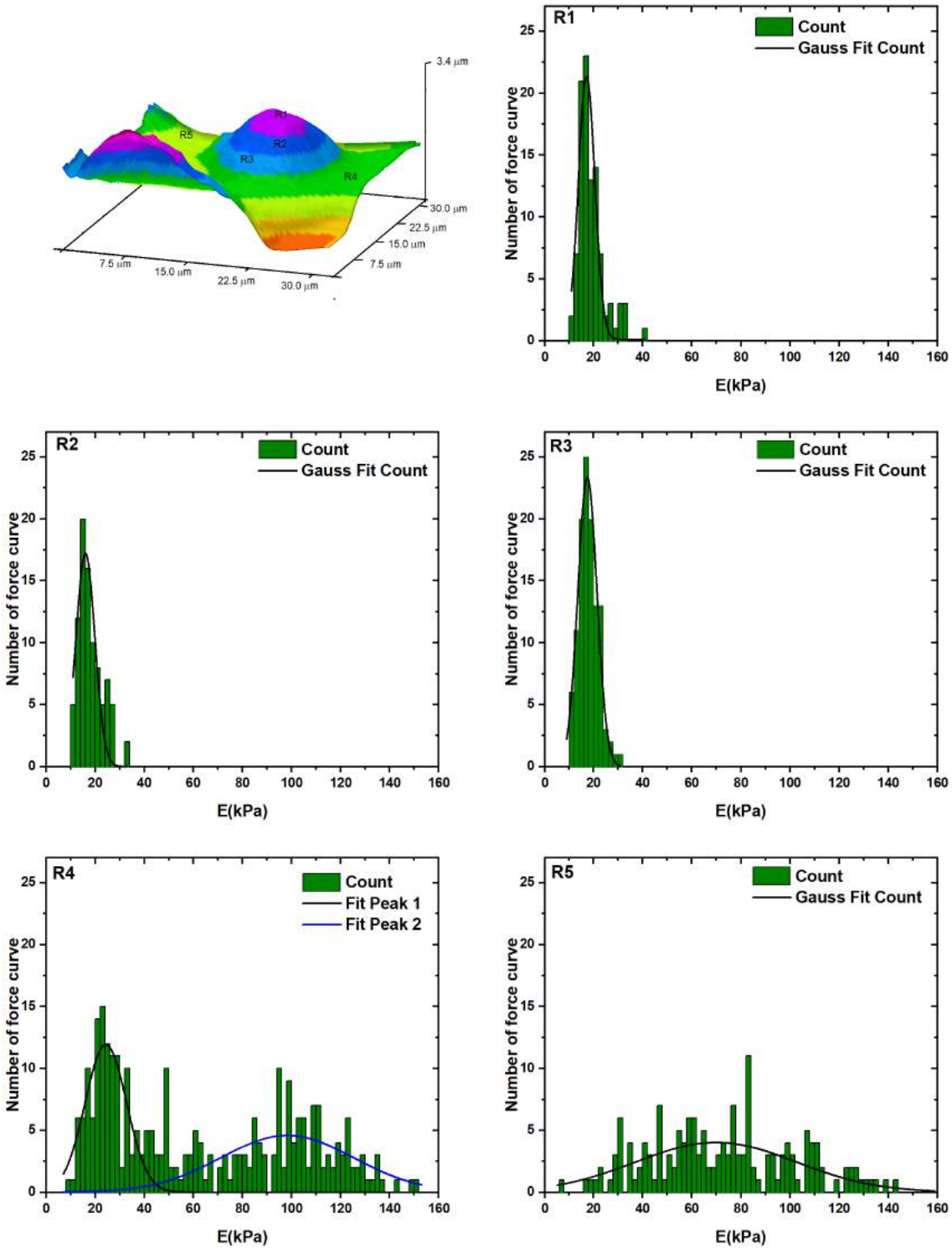

Figure 3.12: Contour image for WM1366 shGal3 cell in 3D, for a better visualization of the cell the scale of the axis z is three times the scale of the axis x and y. The topographic image was sliced in five regions, clearly identified. The histograms associated with each of the regions together with their respective Gaussian settings are also displayed. The scales have been standardized for a correct comparison.

Table 3.2: Summary of the elastic modulus calculated for each cellular region from the Gaussian fitting

Region	**HaCaT (kPa)**	**shSCR (kPa)**	**shGal3 (kPa)**
R1	33.5 ± 0.9	17 ± 1	17.2 ± 0.6
R2	33 ± 2	24 ± 3	15.8 ± 0.6
R3	25 ± 1	28 ± 2	17.5 ± 0.7
	48 ± 4		
R4	33 ± 2	31 ± 2	23.6 ± 0.6
	57 ± 2		97 ± 1
R5	59 ± 4	39 ± 3	70 ± 5

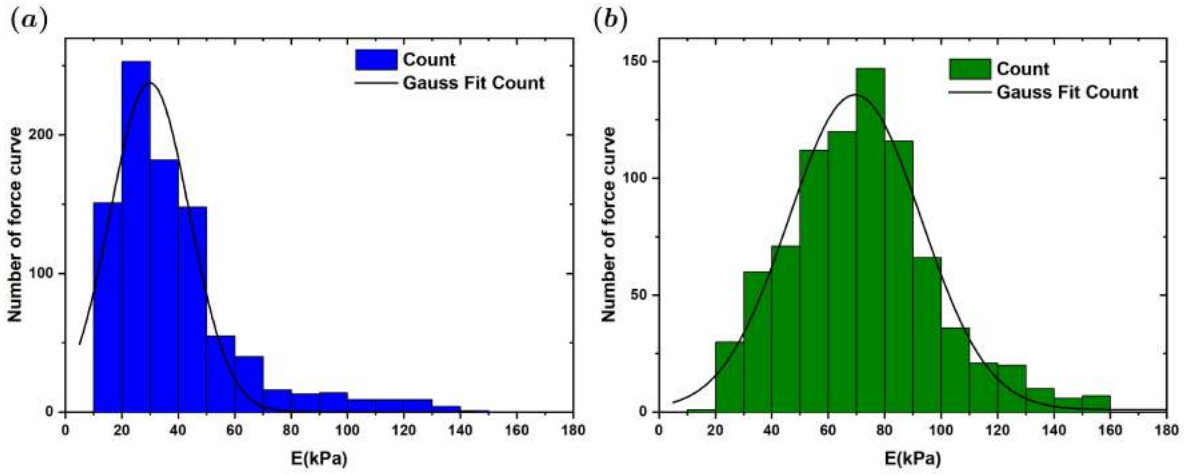

Figure 3.13: Force curves acquired in the peripheral region of 5 cells of (a) WM1366 shSCR and (b) WM1366 shGal3.

4

Conclusions and perspectives

The data shown here reflect the standardization of the conditions to actually measure the elastic modules of cells and the cell:extracellular matrix interface in experimental conditions. The cellular system used included HaCaT keratinocytes cells and the melanoma cell line WM1366 (shSCR), which expresses the endogenous lectin galectin-3 and its counterpart engineered to loose galectin-3 expression (shGal3). Galectin-3 is a matricellular protein produced by a variety of cells (either normal or tumor cells) that is eventually secreted to the extracellular space (Melo et al. [80]; Cardoso et al. [13]). Upon secretion, galectin-3 may act as a lectin interacting with a variety of glycoproteins in the cellular space, such as laminins and collagens. In the presence of galectin-3, the assembly of extracellular matrix molecules is altered. In vivo, dense collagen fibers are formed in the presence of galectin-3, e.g. (Oliveira et al. [81]).

Initially, AFM topographic images were acquired in contact-mode under liquid environment (PBS) of each fixed cell line. It was observed that HaCaT cells exhibit different formats and are characterized by dense filamentous structures in the cell-cell junction regions. Unlike the keratenocyte cells, melanoma WM1366 cells show a more regular format and do not show distinctive morphological features between shSCR and shGal3 cells. In addition, the cell and cell-cell junction regions do not present filamentous structures, as it was observed for HaCaT. From AFM topographic images some height profiles were taken, these show that keratinocyte cells are lower than WM1366 melanoma cells by about 1.0 to 2.0 μm. Also, it was observed that neoplastic cells tend to overlap, which influences notoriously some morphological parameters.

The elasticity measurements made in this study indicated that the elastic modulus of melanoma cells devoid of galectin-3 are significant smaller than those present in melanoma cells expressing galectin-3. More interestingly, the gradient of elastic modules in cells from the nuclear region towards the cell periphery is more pronounced in cells devoid of galectin-3. The increased elastic module in the pericellular region of cells devoid of galectin-3 suggests that the organization of the extracellular matrix in these areas is different than those observed around HaCaT and shSCR WM1366 cells. It is well known that galectin-3 may interfere with matrix assembly, as mentioned above, besides interfering with extracellular matrix remodeling (Lagana et al. [82]; Vijayakumar et al.

[83]; Takemoto et al. [84]; Luo et al. [85]). Regardless, the biological significance of this finding warrants further investigation.

Here the initial conditions to measure the elastic modules in cells were standardized. Future experiments will include analysis of co-cultures between both HaCaT cells and WM cells (either expressing or not galectin-3). Under these conditions, we will mimic the interactions found within a radial growth phase of melanomas, where tumor cells are still interacting with other melanoma cells and keratinocytes. It will be interesting to delineate a map of elastic modules across the surfaces where we find keratinocytes neighbouring other keratinocytes, keratinocytes neighbouring melanoma cells and finally melanoma cells neighbouring melanoma cells. We anticipate a gradient between the distribution observed in Figure 3.3. Biological studies will then enable us to determine how migratory melanoma cells are within the population of keratinocytes and to determine whether the expression of galectin-3 will interfere with the pattern of growth and invasiveness of melanoma cells in co-culture systems.

Bibliography

[1] https://www.webmd.com/melanoma-skin-cancer/guide/skin-cancer#1

[2] http://www2.inca.gov.br/wps/wcm/connect/tiposdecancer/site/home/pele_melanoma/definicao

[3] Weinstein, D., Leininger, J., Hamby, C, Safai B1.Diagnostic and prognostic biomarkers in melanoma.

[4] Bobrowska, J. (2016). Characterization of cell surface structure and its relation to cytoskeleton elasticity in cancer cells. The Henryk Niewodniczański Institute of Nuclear Physics Polish Academy of Sciences. Kraków, Poland.

[5] Jinka, R., Kapoor, R., Sistla, P. G., Raj, T. A., and Pande, G. (2012). Alterations in cellular matrix interactions during progression of cancers. International Journal of Cell Biology, 2012, Article ID 219196, 8 pages.

[6] Lekka, M., Laidler, P., Gil, D., Lekki, J., Stachura, Z., and Hrynkiewicz, A. Z. (1999). Elasticity of normal and cancerous human bladder cells studied by scanning force microscopy, Eur. Biophys. J., 28, pp. 312–316.

[7] Lekka, M. (2016). Discrimination Between Normal and Cancerous Cells Using AFM. BioNanoScience, 6(1), 65–80.

[8] Hochmuth, R. M. (2000). Micropipette aspiration of living cells. Journal of Biomechanics, 33(1), 15–22. doi:10.1016/s0021-9290(99)00175-x

[9] Dao, M., Lim, C. T., and Suresh, S. (2003). Mechanics of the human red blood cell deformed by optical tweezers. Journal of the Mechanics and Physics of Solids, 51(11-12), 2259–2280. doi:10.1016/j.jmps.2003.09.019

[10] Tanase, M., Biais, N., and Sheetz, M. (2007). Magnetic Tweezers in Cell Biology. Cell Mechanics, 473–493. doi:10.1016/s0091-679x(07)83020-2

[11] Laurent, V. M., Hénon, S., Planus, E., Fodil, R., Balland, M., Isabey, D., and Gallet, F. (2002). Assessment of Mechanical Properties of Adherent Living

Cells by Bead Micromanipulation: Comparison of Magnetic Twisting Cytometry vs Optical Tweezers. Journal of Biomechanical Engineering, 124(4), 408. doi:10.1115/1.1485285

[12] Suresh, S. (2007). Biomechanics and biophysics of cancer cells. Acta Biomaterialia, 3(4), 413–438. doi:10.1016/j.actbio.2007.04.002

[13] Cardoso, A. C. F., Andrade, L. N. de S., Bustos, S. O., and Chammas, R. (2016). Galectin-3 Determines Tumor Cell Adaptive Strategies in Stressed Tumor Microenvironments. Frontiers in Oncology, 6. doi:10.3389/fonc.2016.00127

[14] Bustos, S. O., Pereira, G. J. da S., Saito, R. de F., Gil, C. D., Zanatta, D. B., Smaili, S. S., and Chammas, R. (2018). Galectin-3 sensitized melanoma cell lines to vemurafenib (PLX4032) induced cell death through prevention of autophagy. Oncotarget, 9(18). doi:10.18632/oncotarget.24516

[15] Lekka, M. (2017). Cellular Analysis by Atomic Force Microscopy. New York: Pan Stanford.

[16] Xu, W., Mezencev, R., Kim, B., Wang, L., McDonald, J., and Sulchek, T. (2012). Cell Stiffness Is a Biomarker of the Metastatic Potential of Ovarian Cancer Cells. PLoS ONE, 7(10), e46609. doi:10.1371/journal.pone.0046609

[17] Cross, S. E., Jin, Y.-S., Rao, J., and Gimzewski, J. K. (2007). Nanomechanical analysis of cells from cancer patients. Nature nanotechnology 2(12) 780.

[18] Kenete, A. N., Roberts, P. C., Shea, A. A., Schmelz, E. M., and Agah, M. (2012). : Integr. Biol., 4, 540–549

[19] Pullarkat, P., Fernandez, P., and Ott, A. (2007). Rheological properties of the Eukaryotic cell cytoskeleton. Physics Reports, 449(1-3), 29–53. doi:10.1016/j.physrep.2007.03.002

[20] Alberts, B., Bray, D., Lewis, J., Raff, M., Roberts, K., and Watson, J. D. (2002) Molecular Biology of the Cell, Garland Science Publ., NewYork.

[21] Chiou, Y.-W., Lin, H.-K., Tang, M.-J., Lin, H.-H., and Yeh, M.-L. (2013). The Influence of Physical and Physiological Cues on Atomic Force Microscopy-Based Cell Stiffness Assessment. PLoS ONE, 8(10), e77384. doi:10.1371/journal.pone.0077384

[22] Meyers, M. A., Chen, P.-Y., Lin, A. Y.-M., and Seki, Y. (2008). Biological materials: Structure and mechanical properties. Progress in Materials Science, 53(1), 1–206. doi:10.1016/j.pmatsci.2007.05.002

[23] Du, G., Ravetto, A., Fang, Q., and den Toonder, J. M. J. (2010). Cell types can be distinguished by measuring their viscoelastic recovery times using a micro-fluidic device. Biomedical Microdevices, 13(1), 29–40. doi:10.1007/s10544-010-9468-4

[24] S. Suresh, Connections between single-cell biomechanics and human disease states : gastrointestinal cancer and malaria, 1 (2005) 15–30. doi:10.1016/j.actbio.2004.09.001.

[25] Lekka, M., and Laidler, P. (2009). Applicability of AFM in cancer detection. Nature Nanotechnology, 4(2), 72–72. doi:10.1038/nnano.2009.004

[26] Hall, A. (2009). The cytoskeleton and cancer. Cancer and Metastasis Reviews, 28(1-2), 5–14. doi:10.1007/s10555-008-9166-3

[27] Xu, W., Mezencev, R., Kim, R., Wang, L., McDonald, J., and Sulchek, T. (2012). Cell Stiffness Is a Biomarker of the Metastatic Potential of Ovarian Cancer Cells, PLoS One. 7. doi:10.1371/journal.pone.0046609.

[28] Lekka, M., Gil, D., Pogoda, K., Dulinska-Litewka, J., Jach, R., and Gostek, J. (2012). Cancer cell detection in tissue sections using AFM., Arch. Biochem. Biophys. 518 151–6. doi:10.1016/j.abb.2011.12.013.

[29] Rotsch, C., and Radmacher, M. (2000). Drug-Induced Changes of Cytoskeletal Structure and Mechanics in Fibroblasts: An Atomic Force Microscopy Study. Biophysical Journal, 78(1), 520–535. doi:10.1016/s0006-3495(00)76614-8

[30] Rosenbluth, M. J., Lam, W. A., and Fletcher, D. A. (2006). Force Microscopy of Nonadherent Cells: A Comparison of Leukemia Cell Deformability. Biophysical Journal, 90(8), 2994–3003. doi:10.1529/biophysj.105.067496

[31] Hinterdorfer, P., Dufrêne, Y. (2006). Detection and localization of single molecular recognition events using atomic force microscopy. *Nature Methods.* 3, 347-355.

[32] Seo, Y., Jhe, W. (2007). Atomic force microscopy and spectroscopy. Reports on Progress in Physicis, 71(1), 016101.

[33] C. Verdier, J. Etienne, A. Duperray, L. Preziosi, Review: Rheological properties of biological materials, Comptes Rendus Phys. 10 (2009) 790–811. doi:10.1016/j.crhy.2009.10.003.

[34] Sobiepanek, A., et al., Biosensors and Bioelectronics (2016), http://dx.doi.org/10.1016/j.bios.2016.08.088i

[35] Gostek, J., Prauzner-Bechcicki, S., Nimmervoll, B., Mayr, K., Pabijan, J., Hinterdorfer, P., Lekka, M. (2014). Nano-characterization of two closely related melanoma cell lines with different metastatic potential. European Biophysics Journal, 44(1-2), 49–55. doi:10.1007/s00249-014-1000-y

[36] Pogoda, K., Jaczewska, J., Wiltowska-Zuber, J., Klymenko, O., Zuber, K., Fornal, M., and Lekka, M. (2011). Depth-sensing analysis of cytoskeleton organization based on AFM data. European Biophysics Journal, 41(1), 79–87. doi:10.1007/s00249-011-0761-9

[37] Krieg, M., Flaschner, G., Alsteens, D., Gaub, B. M., Roos, W. H., Wuite, G. J. L., and Muller, D. J. (2018). Atomic force microscopy-based mechanobiology. Nature Reviews Physics. doi:10.1038/s42254-018-0001-7

[38] Zemła, J., Danilkiewicz, J., Orzechowska, B., Pabijan, J., Seweryn, S., and Lekka, M. (2018). Atomic force microscopy as a tool for assessing the cellular elasticity and

adhesiveness to identify cancer cells and tissues. Seminars in Cell and Developmental Biology, 73, 115–124. doi:10.1016/j.semcdb.2017.06.029

[39] Lekka, M., Pogoda, K., Gostek, J., Klymenko, O., Prauzner-Bechcicki, S., Wiltowska-Zuber, J., et al. (2012). Cancer cell recognition mechanical phenotype. Micron, 43, 1259–1266.

[40] Li, Q. S., Lee, G. Y., Ong, C. N., Lim, C. T. (2008). AFM indentation study of breast cancer cells. Biochemical and Biophysical Research Communication, 374, 609–613.

[41] P. Abrão Possik. (2008). Estudio do papel de Galectina-3 no fenótipo maligno de células de melanoma primário e metastático. São Paulo.

[42] Bissell, M. J., and Radisky, D. (2001). Putting tumours in context. Nature Reviews Cancer, 1(1), 46–54. doi:10.1038/35094059

[43] Hanahan, D., Weinberg, R. (2000). The Hallmarks of cancer. Cell. Vol. 100, 57-70.

[44] Ciasca, G., Papi, M., Di Claudio, S., Chiarpotto, M., Palmieri, V., Maulucci, G., et al. (2015). Mapping viscoelastic properties of healthy and pathological red blood cells at the nanoscale level. Nanoscale. doi:10.1039/C5NR03145A.

[45] R.O. Hynes, Integrins: versatility, modulation, and signaling in cell adhesion., Cell. 69 (1992) 11–25.

[46] V.D. Criscione, M. a Weinstock, Melanoma thickness trends in the United States, 1988-2006., J. Investig. Dermatologyinvestigative Dermatology. 130 (2010) 793–797.

[47] T. Ochalek, F.J. Nordt, K. Tullberg, M.M. Burger, Correlation between cell deformability and metastatic potential in B16-F1 melanoma cell variants, Cancer Res. 48 (1988) 5124–5128.

[48] Brown ER, Doig T, Anderson N, Brenn T, Doherty V, Xu Y, Bartlett JM, Smyth JF, Melton DW. Association of galectin-3 expression with melanoma progression and prognosis. Eur J Cancer. 2012; 48:865–874.

[49] Li ZW, Wang Y, Xue WC, Si L, Cui CL, Cao DF, Zhou LX, Guo J, Lu AP. [Expression and prognostic significance of galectin-1 and galectin-3 in benign nevi and melanomas]. [Article in Chinese]. Zhonghua Bing Li Xue Za Zhi. 2013; 42:801–805.

[50] Thijssen VL, Heusschen R, Caers J, Griffioen AW. Galectin expression in cancer diagnosis and prognosis: A systematic review. Biochim Biophys Acta. 2015; 1855:235–247.

[51] Ruvolo PP. Galectin 3 as a guardian of the tumor microenvironment. Biochim Biophys Acta. 2016; 1863:427–437.

[52] Paddison, P. J. (2002). Short hairpin RNAs (shRNAs) induce sequence-specific silencing in mammalian cells. Genes and Development, 16(8), 948–958.

[53] Lewis PF, Emerman M. Passage through mitosis is required for oncoretroviruses but not for the human immunodeficiency virus. J Virol. 1994;68(1):510–516.

[54] Buchschacher, G. L., and Wong-Staal, F. (2000). Development of lentiviral vectors for gene therapy for human diseases. Blood, 95(8), 2499-2504

[55] G. Binnig, C. F. Quate, and Ch. Gerber. (1986). *Phys. Rev. Lett.*. **56**, 930.

[56] Piontek M.C., Roos W.H. (2018). Atomic Force Microscopy: An Introduction. In: Peterman E. (eds) Single Molecule Analysis. *Methods in Molecular Biology*, vol 1665 Humana Press, New York, NY.

[57] Eaton, P., West, P. (2014). Atomic Force Microscopy. Oxford University Press.

[58] Radmacher, M., Tillamnn, R. W., Fritz, M., and Gaub, H. E. (1992) From molecules to cells: imaging soft samples with the atomic force microscope. Science (New York, N.Y.) 257(September).

[59] Henderson, E., Haydon, P., and Sakaguchi, D. (1992). Actin filament dynamics in living glial cells imaged by atomic force microscopy. Science 257(5078).

[60] Müller, D. J. and Engel, A. (2007). Atomic force microscopy and spectroscopy of native membrane proteins. Nature protocols 2(9) 2191.

[61] Braet F., Seynaeve C., De Zanger R., Wisse E. (1998). Imaging surface and submembranous structures with the atomic force microscope: a study on living cancer cells, fibroblasts and macrophages. J Microsc. 1998 Jun;190(Pt 3):328-38.

[62] Rigato, A. (2015). Characterization of cell mechanics with atomic force microscopy: mechanical mapping and high-speed microrheology,. Aix-Marseille Université. Ecole Doctorale de Sciences de la Vie et de la Santé. Specialité: Biologie. France.

[63] Carvalho, F. A., Santos, N.C. (2012). Atomic force microscopy-based force spectroscopy-biological and biomedical applications. IUBMB Life 64,(6), 465-472.

[64] Hertz, H. (1882). On the contact of elastic bodies, volume In Hertz's Miscellaneous Papers. Macmillan, London.

[65] Sneddon, I. N. (1965). The relation between load and penetration in the axisymmetric boussinesq problem for a punch of arbitrary profile. International Journal of Engineering Science 3(1) 47.

[66] Bilodeau, G. G. (1992). Regular Pyramid Punch Problem. Journal of Applied Mechanics 59(3) 519.

[67] Matzke, R.,Jacobson,K.,Radmacher,M.(2001).Nature Cell Biology 3, 607–610.

[68] Hermanowicz, P., Sarna, M., Burda, K., and Gabryś, H. (2014). AtomicJ: An open source software for analysis of force curves. Review of Scientific Instruments, 85(6), 063703. doi:10.1063/1.4881683

[69] Radmacher, M. (1997). Measuring the elastic properties of biological samples with the AFM. IEEE Engineering in Medicine and Biology Magazine, 16(2), 47–57. doi:10.1109/51.582176

[70] Gavara, N. (2016). A beginner's guide to atomic force microscopy probing for cell mechanics. Microscopy Research and Technique, 80(1), 75–84.

[71] Kobiela, T., Lelen-Kaminska, K., Stepulak, M., Lekka, M., Malejczyk, M., Arct, J., and Majewski, S. (2012). The influence of surfactants and hydrolyzed proteins on keratinocytes viability and elasticity. Skin Research and Technology, 19(1), e200–e208. doi:10.1111/j.1600-0846.2012.00628.x

[72] MultiMode Instruction Manual. (2011) Bruker.

[73] Kroeger, M. E., Sorenson, B. A., Thomas, J. S., Stojkovic, E. A., Tsonchev, S., and Nicholson, K. T. (2014). Atomic Force Microscopy of Red-Light Photoreceptors Using PeakForce Quantitative Nanomechanical Property Mapping. Journal of Visualized Experiments, (92). doi:10.3791/52164

[74] Gavara, N., and Chadwick, R. S. (2015). Relationship between cell stiffness and stress fiber amount, assessed by simultaneous atomic force microscopy and live-cell fluorescence imaging. Biomechanics and Modeling in Mechanobiology, 15(3), 511–523.

[75] Haydon, P. G., Lartius, R., Parpura, V., and Marchese-Ragona, S. P. (1996). Membrane deformation of living glial cells using atomic force microscopy. Journal of Microscopy, 182(2), 114–120.

[76] Hutter, J. L., and Bechhoefer, J. (1993). Calibration of atomic force microscope tips. Review of Scientific Instruments, 64(7), 1868–1873.

[77] Salvadori, M. C., Araújo, W. W. R., Teixeira, F. S., Cattani, M., Pasquarelli, A., Oks, E. M., and Brown, I. G. (2010). Termination of diamond surfaces with hydrogen, oxygen and fluorine using a small, simple plasma gun. Diamond and Related Materials, 19(4), 324–328. doi:10.1016/j.diamond.2010.01.002

[78] Guo, Q., Xia, Y., Sandig, M., and Yang, J. (2012). Characterization of cell elasticity correlated with cell morphology by atomic force microscope. Journal of Biomechanics, 45(2), 304–309. doi:10.1016/j.jbiomech.2011.10.031

[79] Wang, X., Bleher, R., Brown, M. E., Garcia, J. G. N., Dudek, S. M., Shekhawat, G. S., and Dravid, V. P. (2015). Nano-Biomechanical Study of Spatio-Temporal Cytoskeleton Rearrangements that Determine Subcellular Mechanical Properties and Endothelial Permeability. Scientific Reports, 5(1). doi:10.1038/srep11097

[80] Melo FH, Butera D, Junqueira Mde S, Hsu DK, da Silva AM, Liu FT, Santos MF, Chammas R. The promigratory activity of the matricellular protein galectin-3 depends on the activation of PI-3 kinase. PLoS One. 2011;6(12):e29313. doi:10.1371/journal.pone.0029313. Epub 2011 Dec 28. PubMed PMID: 22216245; PubMed Central PMCID: PMC3247242.

[81] Oliveira FL, Frazão P, Chammas R, Hsu DK, Liu FT, Borojevic R, Takiya CM, El-Cheikh MC. Kinetics of mobilization and differentiation of lymphohematopoietic cells during experimental murine schistosomiasis in galectin-3 mice. J Leukoc Biol. 2007 Aug;82(2):300-10. Epub 2007 Apr 24. PubMed PMID: 17456800.

[82] Lagana A, Goetz JG, Cheung P, Raz A, Dennis JW, Nabi IR. Galectin binding to Mgat5-modified N-glycans regulates fibronectin matrix remodeling in tumor cells.

Mol Cell Biol. 2006 Apr;26(8):3181-93. PubMed PMID: 16581792; PubMed Central PMCID: PMC1446937.

[83] Vijayakumar S, Peng H, Schwartz GJ. Galectin-3 mediates oligomerization of secreted hensin using its carbohydrate-recognition domain. Am J Physiol Renal Physiol. 2013 Jul 1;305(1):F90-9. doi:10.1152/ajprenal.00498.2012. Epub 2013 May 8. PubMed PMID: 23657851; PubMed Central PMCID: PMC3725678.

[84] Takemoto Y, Ramirez RJ, Yokokawa M, Kaur K, Ponce-Balbuena D, Sinno MC, Willis BC, Ghanbari H, Ennis SR, Guerrero-Serna G, Henzi BC, Latchamsetty R, Ramos-Mondragon R, Musa H, Martins RP, Pandit SV, Noujaim SF, Crawford T, Jongnarangsin K, Pelosi F, Bogun F, Chugh A, Berenfeld O, Morady F, Oral H, Jalife J. Galectin-3 Regulates Atrial Fibrillation Remodeling and Predicts Catheter Ablation Outcomes. JACC Basic Transl Sci. 2016 Apr;1(3):143-154. PubMed PMID: 27525318; PubMed Central PMCID: PMC4979747.

[85] Luo H, Liu B, Zhao L, He J, Li T, Zha L, Li X, Qi Q, Liu Y, Yu Z. Galectin-3 mediates pulmonary vascular remodeling in hypoxia-induced pulmonary arterial hypertension. J Am Soc Hypertens. 2017 Oct;11(10):673-683.e3. doi:10.1016/j.jash.2017.07.009. Epub 2017 Jul 28. PubMed PMID: 28826890.